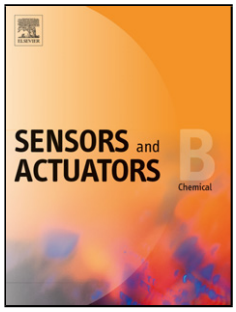

Title: Humidity sensing properties of nanocrystalline pseudobrookite (Fe_2TiO_5) based thick films

Authors: Maria Vesna Nikolic, Zorka Z. Vasiljevic, Miloljub D. Lukovic, Vera P. Pavlovic, Jelena Vujancevic, Milan Radovanovic, Jugoslav B. Krstic, Branislav Vlahovic, Vladimir B. Pavlovic

PII: S0925-4005(18)31683-6
DOI: https://doi.org/10.1016/j.snb.2018.09.063
Reference: SNB 25369

To appear in: *Sensors and Actuators B*

Received date: 15-5-2018
Revised date: 23-8-2018
Accepted date: 15-9-2018

Please cite this article as: Nikolic MV, Vasiljevic ZZ, Lukovic MD, Pavlovic VP, Vujancevic J, Radovanovic M, Krstic JB, Vlahovic B, Pavlovic VB, Humidity sensing properties of nanocrystalline pseudobrookite (Fe_2TiO_5) based thick films, *Sensors and Actuators: B. Chemical* (2018), https://doi.org/10.1016/j.snb.2018.09.063

Humidity sensing properties of nanocrystalline pseudobrookite (Fe_2TiO_5) based thick films

Maria Vesna Nikolic[1*], Zorka Z. Vasiljevic[2], Miloljub D. Lukovic[1], Vera P. Pavlovic[3], Jelena Vujancevic[2], Milan Radovanovic[4], Jugoslav B. Krstic[5], Branislav Vlahovic[6], Vladimir B. Pavlovic[2]

[1]Institute for Multidisciplinary Research, University of Belgrade, Kneza Viseslava 1, 11030 Belgrade, Serbia
[2]Institute of Technical Sciences of the Serbian Academy of Sciences and Arts (SASA), Knez Mihailova 35, Belgrade, Serbia
[3]University of Belgrade, Faculty of Mechanical Engineering, Belgrade, Serbia
[4]University of Novi Sad, Faculty of Technical Sciences, Novi Sad, Serbia
[5]Institute of Chemistry, Technology and Metallurgy, Department of Catalysis and Chemical Engineering, University of Belgrade, Belgrade, Serbia
[6]North Carolina Central University, Durham NC 27707, USA

*mariav@rcub.bg.ac.rs

Graphical abstract

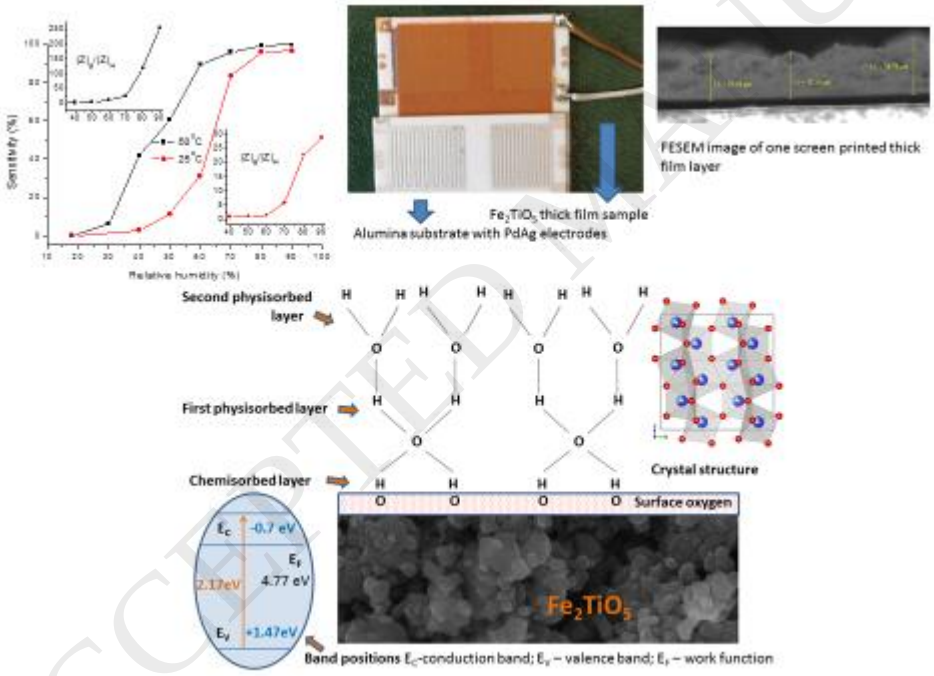

Highlights

- Nanocrystalline pseudbrookite thick films
- High humidity sensing
- Fast response
- Short time delay

Abstract

Pseudobrookite based nanopowder was obtained by solid state synthesis of starting hematite and anatase nanopowders in the weight ratio 55:45. Structural and morphological properties were analyzed using X-ray diffraction (XRD), BET, X-ray photoelectron spectroscopy (XPS), Raman spectroscopy, UV/Vis diffuse reflectance spectroscopy, Field emission scanning electron microscopy (FESEM) and Transmission electron microscopy (TEM) confirming the formation of nanocrystalline pseudobrookite. The obtained powder was mixed with a binder (ethyl cellulose), dispersant (α-terpinol) and adhesion agents (acetic acid and distilled water) to obtain a thick film paste. It was screen printed on alumina substrate with interdigitated PdAg electrodes and fired at 600^{o}C for 30 minutes. Formation of a porous nanocrystalline thick film structure was shown using Scanning electron microscopy (SEM), while Hall measurements enabled determination of carrier mobility. Change of impedance response in the frequency range 42 Hz - 1 MHz with humidity was analyzed at room temperature (25^{o}C) and 50^{o}C in the relative humidity range 30-90% and 40-90%, respectively. At 42 Hz, and room temperature the impedance reduced ~28 times, while at 50^{o}C it reduced ~147 times in the relative humidity range 40-90%. The sensor showed rapid response (16 s) and relatively low hysteresis (8.39% at 25^{o}C and 2.64% at 50^{o}C) showing that this is a promising material for application in humidity sensing.

Keywords: Pseudobrookite**,** Fe_2TiO_5**,** humidity sensor; thick film

1. Introduction

With water being one of the essential components on Earth it remains significant to enable reliable and accurate measurement of the water content [1]. Ceramic humidity sensors are widely investigated and applied as they have good thermal and environmental stability, response and mechanical strength, wide range of operating temperatures, low fabrication cost, robustness and selectivity towards a wide range of gases [1, 2]. As such they satisfy many of the basic requirements of a good gas sensor [1]. Metal oxide semiconductor materials are most commonly used in ceramic humidity sensors [3]. These include metal oxides such as ZnO, TiO_2, Fe_2O_3 [1, 3], spinel oxides [4] or perovskite type oxides [5]. However, for instance, pure Fe_2O_3 suffers from low sensitivity therefore there is a need for new materials. With the advent of nanotechnology, nanostructured metal oxides emerge as one of the most fascinating functional materials [3]. Nanostructured metal oxide gas sensors can be constructed with a small size, controlled morphology and electrical characteristics that have resulted in optimized sensing characteristics [1]. As small size and high surface area supply more active sites for water vapor, better performance in humidity sensing would be provided. Also, the porous structure of ceramic materials consisting of grains, grain boundaries, surface areas and pores influence the sensor performance [1].

Pseudobrookite is an iron-titanium oxide with the general formula $Fe_{2-x}Ti_{1+x}O_5$, ranging from ferric Fe_2TiO_5 (x=0) to ferrous $FeTi_2O_5$ (x=1) pseudobrookite [6, 7]. It normally crystallizes into a *Cmcm* orthorhombic crystal structure. Its band gap is ~2.2 eV, similar to hematite [8]. In the continued search for a good photoelectrode material combination, in recent literature, Fe_2TiO_5 figures often [8-10]. In our previous work we investigated the humidity sensing potential of pseudobrookite in bulk form [11]. In this work we have focused on analyzing humidity sensing of nanostructured pseudobrookite based thick films by monitoring the change in impedance in conditions of enhanced humidity (relative humidity 30-90%).

2. Experimental

2.1 Synthesis of pseudobrookite nanoparticles and thick film preparation

Hematite, α-Fe_2O_3 (Alfa Aesar, 99%, grain size 20–60 nm) and anatase, TiO_2, (Alfa Aesar, 99.7%, grain size 15 nm) nanopowders in the weight ratio 55:45, were ball milled in a planetary mill (Fritsch Pulversisette 5) in stainless steel vessels with stainless steel balls for 60 min, followed by drying at 150 °C for 24 h. The obtained powder was calcined in air at 900 °C for 2 h and then sieved through a 400 mesh sieve. Thick film paste was prepared by the addition of organic agents (a-terpineol (95% min, Alfa Aesar) as a dispersant, ethyl-cellulose (viscosity 4 cP, Aldrich Chemistry) as a binder, and the combination of acetic acid (MOS HEMOS, pro analysi) and distilled water as adhesion agents and homogenized using the ultrasonic horn (Bandelin Sonoplus 2070HD) following the procedure reported by Ito et al [12].

Samples for Hall measurements were prepared by screen printing 3 layers of pseudobrookite thick film paste on alumina substrate. Samples for electrical and humidity sensing characterization were made by first screen printing interdigitated PdAg electrodes on alumina substrate, followed by firing in a conveyor furnace at 850ºC for 10 minutes in air. The analyzed electrode spacing was 0.25 mm (as shown in Fig. 1). Two to five layers of pseudobrookite based thick film paste were then screen printed on the prepared alumina substrate with interdigitated PdAg electrodes. Each layer was dried for 15 minutes at 60ºC, before the next layer was printed. The average layer thickness was estimated to be 12-15 µm. The sensors were heat treated in air in a chamber furnace at 600ºC for 30 minutes. An example of a thick film test sample is shown in Fig. 1.

2.2 Characterization of pseudobrookite nanoparticles and thick film samples

The crystal structure of the synthesized pseudobrookite nanopowder was investigated by X-Ray diffraction (XRD). XRD patterns were recorded on a Philips PW1050 diffractometer equipped with Cu Kα radiation and operating in a 2θ range of 10 to 90º, step 0.05s and hold time 10s. The structural parameters were refined using the Rietveld method and the GSAS II package [13].

Raman spectra were recorded using a He-Ne laser (632.8 nm) on a Horiba Jobin Yvon LabRam HR Evolution spectrometer in a backscattering geometry, range 100-1500 cm^{-1}, power at sample 0.4 mW.

The chemical states of the elements were determined with X-ray photoelectron spectra (XPS) on a Kratos Axis Ultra XPS system. The X-Ray source was monochromated Aluminum K-alpha X-Ray with a source voltage of 15 kV and current of 10 mA. All survey scans were performed with pass energy of 160 eV, and all region scans were performed with pass energy of 20 eV. All data was calibrated to the C-C portion of the C1s peak at 284.5 eV.

The morphology and microstructure were analyzed by Field Emission Scanning Electron Microscopy (FESEM) on a Tescan MIRA3 XM FESEM device (powder and thick film samples) and Transmission electron microscopy (TEM) on a JEOL JEM-1400 PLUS device (powder sample) and Scanning electron microscopy (SEM) on a TESCAN Electron Microsope VEGA TS 5130MM device (thick film samples).

Nitrogen adsorption-desorption isotherms of pseudobrookite powder were collected on a Sorptomatic 1990 Thermo Finningen at 77 K. The specific surface area (m^2/g) was calculated from the obtained isotherm using the Brunauer-Emmett-Teller (BET) equation. The pore size was evaluated using the Barrett-Joyner-Halenda (BJH) method.

UV/vis diffuse reflectance spectra of the obtained powder were measured on a Shimadzu UV-2600 with an ISR2600 Plus Integrating sphere attachment in the measuring range 200-1200 nm.

Hall measurements were conducted at room temperature (300 K) and 77 K on an Ecopia HMS-3000 Hall effect measurement system with applied field of 0.37 (300 and 77 K) and 1 T (300K), with varied input currents of 1, 3 and 5 nA.

2.3 Humidity sensing characterization

Electrical characterization was performed in a JEIO TECH TH-KE-025 Temperature and humidity climatic chamber by measuring impedance in the frequency range 42 Hz - 1MHz on a HIOKI 3532-50 LCR HiTESTER device at 25^{o}C (average room temperature) in the relative humidity (RH) range 40-90% and at 50^{o}C (slightly elevated temperature) in the relative humidity range 30-90% (Fig. 2). Prior to each measurement the samples were dried/heated for 20 minutes at 50^{o}C to remove any moisture. The test sample was placed into the chamber and the electrical properties were measured using wires soldered to the electrodes. The desired temperature and humidity values were obtained by setting the control of the temperature and humidity chamber to the desired temperature first and when this was established (depending on the ambient temperature this took on average about 30 minutes to achieve truly stable temperature values) the humidity was varied between 30 and 90%, by setting the desired humidity value (it took on average 45-90 minutes to establish the desired humidity value i.e. saturation to be reached).

3. Results and Discussion

3.1 Structural and morphological properties of Fe_2TiO_5 based nanopowder

XRD analysis showed that powder samples consisted of orthorhombic pseudobrookite (Fe_2TiO_5) as a main phase (56.3 wt%), smaller amounts of hematite (Fe_2O_3 – 19.7 wt%) and rutile (TiO_2 – 22.4 wt%), and a trace of remaining anatase (TiO_2 – 1.6 wt%). Fig. 3 shows the measured powder diffractogram and Rietveld analysis (*wR* 2.7%). The structural parameters of pseudobrookite were refined on the basis of the *Cmcm* space group assuming a random distribution of TiO_6 and FeO_6 octahedra [7, 9]. The unit cell parameters determined for orthorhombic pseudobrookite (Fe_2TiO_5) and atomic positions and determined unit cell parameters for hematite, rutile and anatase are given in Table 1.

Analysis of the measured Raman spectra of the powder sample (Fig. 4) showed that beside modes of orthorhombic pseudobrookite (ID R140974 spectra from the RRUFF database), there are modes of unreacted hematite (ID R050300 spectra from the RRUFF database), two modes of rutile (E_g mode at ~ 440 cm^{-1} and A_{1g} mode at ~ 607 cm^{-1}) and the peak at 148 cm^{-1} which can be assigned to the strongest mode of unreacted anatase [14-16]. A weak B_{1g} mode from rutile that is expected at ~ 142-144 cm^{-1} can partially contribute to the peak at 148 cm^{-1}, but anatase contribution to that peak is dominant (the latter follows from the fact that there is no shifting of the peak to lower wavelength values). It can be therefore concluded that during synthesis of pseudobrookite most anatase transformed to rutile, but some remained, confirming XRD analysis. Modes belonging to unreacted hematite were determined as: A_{1g} mode which in superposition with one of the two strongest modes of pseudobrookite gives the peak at ~ 221 cm^{-1}, E_g modes at: 289 cm^{-1}, 403 cm^{-1} and ~610 cm^{-1} (shoulder), a shoulder at 818 cm^{-1} and a wide mode at ~1307 cm^{-1} resulting from second-order scattering (LO phonon overtone of hematite) [17, 18]. Mode positions belonging to orthorhombic pseudobrookite are in accordance with previously reported data [19-21].

XPS spectrum of the synthesized powder (P1) is shown in Fig. 5a. High resolution XPS peaks of Fe2p, Ti2p and O1s are presented in Figure 5b-d. Positions of Fe2p peaks at 711.9 eV ($Fe2p_{3/2}$) and 725.6 eV ($Fe2p_{1/2}$), as well as the occurrence of a satellite peak at 719.4 eV, reveal that Fe is present as Fe^{3+} in the sample [22, 23]. Peaks belonging to Ti^{4+} in Fe_2TiO_5 are shown in Fig. 5c [23-25]. In the O1s spectrum (Fig. 5d) an asymmetric peak is observed, which can be divided into three peaks: one at 529.9 eV that is assigned to lattice oxygen binding O^{2-}, and two peaks at 531 eV and 532.7 eV that could be assigned to the surface adsorbed oxygen species (hydroxyl-like groups, C-O and O-C=O) [26, 27].

To confirm formation of Fe_2TiO_5 mesoparticles, the XPS valence band (VB) spectra and UV/vis diffuse reflectance spectra of Fe_2TiO_5 were investigated. As shown in Fig. 5e, the valence band maximum binding energy (VBM) of Fe_2TiO_5 is +1.47 eV. The optical band gap was calculated from the measured diffuse reflectance spectrum using the Tauc model [28] for a direct system, as described in detail in [10]. The equivalent absorption coefficient was calculated from the Kubelka-Munk function. The direct band gap was determined as 2.17 eV, as shown in Fig. 6. Hence, the energy level of the conduction band minimum (CBM) of Fe_2TiO_5 is -0.7 eV, which is in accordance with previously reported results [24]. The position of absorption edges was obtained from analysis of the first derivative of the diffuse reflectance spectra (shown as inset on Fig. 6). It consisted of three transition energies, with the most prominent value of transition energy of 2.14 eV being representative of the overall band gap energy and 2.72 and 1.80 eV representing additional energies within the band gap, in accordance with values obtained in [10].

FESEM and TEM were used to investigate surface morphology of Fe_2TiO_5 based powder as displayed in Fig. 7. The top view FESEM images show a quasi-sphere like morphology with an average diameter 60-300 nm. Combined with TEM observation it can be confirmed that as prepared Fe_2TiO_5 mesoparticles are formed as domains consisting of agglomerates.

The BET surface area of pseudobrookite nanoparticles was 12.3 m^2/g, while the maximum pore diameter was 46.4 nm.

3.2 Thick film microstructure and carrier mobility

SEM and FESEM images of the thick film surface shown in Fig. 8 revealed that thick film samples were made of a porous network of aggregated nanoparticles. The size of nanocrystalline grains is in the range of 80-140 nm. A number of voids can also be seen that according to Lee at al [29] suggest the presence of a highly porous network.

Hall effect measurements with an input current of 1 nA and applied field of 0.37 T at room temperature (300 K) enabled determination of: mobility μ=143.4 $cm^2/V{\cdot}s$, carrier density $N_b = 1.473{\cdot}10^9$ cm^{-3}, resistivity $\rho = 2.955{\cdot}10^7$ $\Omega{\cdot}cm$ and average Hall coefficient $4.239{\cdot}10^9$ cm^3/C. At 77 K the mobility increased to 248.5 $cm^2/V{\cdot}s$, carrier density was $N_b = 9.104{\cdot}10^8$ cm^{-3}, resistivity $\rho = 2.759{\cdot}10^7$ $\Omega{\cdot}cm$ and average Hall coefficient $6.857{\cdot}10^9$ cm^3/C The mobility obtained for pseudobrookite thick film is quite high and compared to the value of 6.32 $cm^2/ V{\cdot}s$ obtained by Bassi et al. [30] and values of 1.53 $cm^2/V{\cdot}s$ obtained by Shinde at al. for hematite α-Fe_2O_3 thin films [31] and 0.36 $cm^2/V{\cdot}s$ for anatase thin films by Jeong et al [32].

3.3 Humidity sensing response

The best sensor response (change in impedance) was obtained for the pseudobrookite based thick film samples printed with five layers of pseudobrookite based thick film paste (estimated thick film thickness ~ 60 µm). In the analyzed frequency range 42 Hz-1 MHz the measured impedance decreased with increase in frequency as shown in Fig. 9. With increase in humidity at 25ºC the impedance decreased from 37.11 MΩ measured at 42 Hz for relative humidity (RH) of 40% to 1.32 MΩ for RH 90%. Thus, the impedance reduced ~ 28 times. At the higher operating temperature of 50ºC the measured impedance at 42 Hz reduced from 30.79 MΩ for RH 30%, 19.06 MΩ at RH 40% to 0.129 MΩ at RH 90%. Thus, the impedance reduced ~238 times in the RH range 30-90% and ~147 times in the RH range 40-90%. The change of impedance at 42 Hz and 101 Hz with humidity at 25 and 50ºC is shown in Fig. 10. The increase in operating temperature to 50ºC resulted in overall lower measured impedances.

The sensor response (sensitivity - *S*) is usually defined as the change in resistance of the material on exposure to gas [3]. It can be represented in different forms as: $S = R_a/R_g$; $S = R_g/R_a$; $S = \Delta R/R_g$ or $S=\Delta R/R_a$, where $\Delta R=|R_a-R_g|$, R_a is the sensor resistance in ambient air and R_g is the sensor resistance in the target gas [3]. Zhu et al. [33] analyzed the sensor response of Fe_2TiO_5 tube like nanostructures to ethanol as $S = R_a/R_g$. In our previous work [11] we determined the sensor response of Fe_2TiO_5 bulk samples as:

$$S = \frac{|Z|_{LH} - |Z|_H}{|Z|_{LH}} \times 100 \quad [1]$$

where $|Z|_{LH}$ is the impedance measured at the lowest analyzed humidity and $|Z|_H$ is the impedance measured for different humidity values in the chamber. The calculated sensitivity using eq. [1] for pseudobrookite (Fe_2TiO_5) samples at 25 and 50°C at the frequency of 42 Hz measured in the relative humidity range 30-90% and 40-90%, respectively are shown in Fig. 11. With increase in humidity the sensitivity increases, more slowly at room temperature (25°C) compared to the slightly higher operating temperature of 50°C. As for higher relative humidity values the measured impedance decreased to values that were several magnitudes lower than the starting impedance, we have shown the ratio between the starting sensor impedance ($|Z|_a$) and the sensor impedance at a certain humidity ($|Z|_H$) as insets in Fig. 11. This characteristic shows the sensor response behavior reflecting the significant reduction in impedance at higher relative humidity values (above 70% at 25°C and 60% at 50°C).

3.4 Humidity sensing mechanism

Interaction of Fe_2TiO_5, a metal-oxide n-type semiconductor, with water molecules (humidity) can be described by two basic processes: chemisorption and physisorption [1, 2, 5, 11]. A schematic illustrating of the humidity sensing mechanism of pseudobrookite thick films is shown in Fig. 12. Active sites on the thick film surface start to retain water molecules when exposed to humidity, forming a chemisorbed layer of hydroxides. Significant energy is required for hopping transfer of protons between hydroxyl groups so the measured impedance is high. With further increase in humidity water molecules are physically adsorbed forming a double hydrogen bond. High electrostatic fields in the chemisorbed layer enable easy dissociation of physisorbed water to form hydronium ions. Further increase in humidity leads to the formation of multilayers of physisorbed water molecules onto available oxygen sites by single hydrogen bonding that enables mobility of water molecules. Additional increase in humidity leads to dissociation of hydronium that accepts one proton and releases another proton to neighboring water molecules forming a liquid-like network. In high humidity conditions protons move freely along the water layer. Physisorbed water layers behave like a normal condensed liquid, as low energy is required for proton hopping. This results in an increase in ionic conductivity that can be explained by the Grotthus charge mechanism [35].

As mentioned above, the structure of ceramic materials generally influences the sensing mechanism. In our case, microstructure analysis of pseudobrookite thick films has shown a porous structure consisting of interconnected agglomerates composed of small nanograins (Fig. 8). The slope of the change of measured impedance with increase in humidity (as shown in Fig. 10) and sensor response (sensitivity) shown in Fig. 11, reflects the advance of processes composing the humidity sensing mechanism.

3.5 Response and recovery time

The response time of a sensor is the time a sensor reaches 90% of the total response when exposed to the target gas (in this case moisture), while recovery is the time required for a sensor to return to 90% of the original baseline signal, when the gas/moisture is removed [3]. We measured the response and recovery times of our pseudobrookite based thick film samples to relative humidity of 90% at 100 Hz and at room temperature (25°C). Samples

were inserted into the chamber which had previously reached equilibrium for the set RH of 90%. After reaching the final impedance value in response to RH 90% samples were removed from the chamber and their recovery was measured. The average response time was ~16 s, while the recovery time was very fast and the sensor recovered in ~1 s, as shown in Fig. 13. The difference in response and recovery times can be explained by the microstructure of pseudobrookite thick films (Fig. 8) that consisted of a porous network of aggregated nanoparticles. In accordance with the determined specific surface of pseudobrookite based powder by BET (12.3 m^2/g), internal porosity is relatively low compared to the number and volume of pores between agglomerates, so water vapors do not get trapped into small disordered pores. Thus, desorption when the sensor is removed from the climatic chamber is undisturbed as water vapors exit the porous voids between agglomerates.

3.6 Hysteresis

The time delay between absorption (condensation) and desorption (evaporation) processes represents the hysteresis curve of a sensor and can occur due to disordered mesoporous solids [36]. Hysteresis curves measured at 42 Hz for pseudobrookite based thick film samples at 25 and 50^{o}C are shown in Fig. 14 and was calculated as 8.39% and 2.64%RH, respectively. The time delay was slightly higher at room temperature, compared to the time delay at 50^{o}C with the larger time delay occurring at lower humidity and higher measured impedance. It was similar to the time delay we obtained for bulk pseudobrookite samples [11] and other thick film humidity sensors [5, 37].

3.7 Complex impedance analysis

Complex impedance plots obtained for pseudobrookite based thick film samples are shown in Fig. 15. Similar curves in the shape of part of a depressed semicircular arc were obtained for both analyzed operating temperatures. The semicircles shrank, showing more of the semicircle with increase in humidity in correlation with the described humidity sensing mechanism. The conductivity of ceramic semiconducting materials is at temperatures below 100^{o}C due to a combination of both electronic and ionic conductivity as described in detail by Faharani et al in ref [2]. As increase in humidity leads to physisorption besides chemisorption and further increase in relative humidity to the formation of multilayers of physisorbed water, ionic conductivity explained by the Grotthus charge mechanism becomes the dominant conducting mechanism. Electrolytic conductivity occurs simultaneously with ionic conductivity at high humidity when liquid water condenses into pores according to Kelvin's law [38]. Proof for the existence of both ionic and electrolytic conduction at high relative humidity levels can be obtained from analysis of complex impedance spectra. The change in the shape of the spectra with change/increase in relative humidity reflects the influence of ionic and electrolytic conduction. Some authors were able to separate these influences and showed which one was dominant for different humidity values using a more complex equivalent circuit [5, 38].

The measured impedance data was analyzed with the EIS Spectrum Analyzer Software [39] using an equivalent circuit composed of the dominant grain boundary component represented with a parallel resistance and constant phase element (CPE), shown in Fig. 15. The CPE element was used to replace the capacitor, as described in detail in [11, 40]. The applied equivalent circuit reflected the combined influence of different conduction mechanisms. The determined grain boundary resistance (Fig. 16a) was high for low humidity (232 MΩ for RH 40% at 25^{o}C and 110 MΩ for RH 30% at 50^{o}C) and rapidly decreased as the relative humidity decreased (for example, 66 MΩ for RH 50% at 25^{o}C) with 0.6 and 0.1 MΩ for RH 90% at 25 and 50^{o}C, respectively. The grain boundary relaxation frequency increased with increase in relative humidity, as shown in Fig. 16b. The determined grain

boundary capacitance did not change with relative humidity and was in the range 102-112 pF at 25°C and 122-128 pF at 50°C.

4. Conclusion

In this work we have investigated humidity sensing properties of nanocrystalline pseudobrookite based thick films. Pseudobrookite based nanocrystalline powder was obtained by solid state synthesis of starting hematite and anatase nanopowders. XRD, BET, XPS, Raman spectroscopy, UV/Vis diffuse reflectance spectroscopy, FESEM and TEM confirmed the formation of nanocrystalline orthorhombic pseudbrookite powder with excess hematite, rutile and traces of anatase. The crystallite size was 42 nm. Thick film paste was obtained by mixing the obtained powder with a binder, dispersant and adhesion agents, and screen printed on alumina substrate with interdigitated electrodes (electrode spacing 0.25mm). FESEM and SEM analysis of the thick film surface and cross-section confirmed the formation of a porous structure with grain size in the range 80-140 nm. Hall effect measurements enabled determination of carrier mobility as μ=143.4 $cm^2/V{\cdot}s$. The increase in humidity at both analyzed operating temperatures led to a noticeable decrease in impedance, especially at relative humidity above 60% in accordance with changes in the humidity sensing mechanism (chemisorption, physisorption and the Grotthuss charge mechanism). Complex impedance semicircle arcs were shrinking noticeably with increased water vapors. Modeling with an equivalent circuit confirmed the dominant influence of the grain boundaries, with the determined grain boundary resistance decreasing and relaxation frequency increasing with increase in relative humidity, while the grain boundary capacitance did not change.

Acknowledgement

The authors would like to express their gratitude to Dr. M. Mitrić for XRD measurements, Dr. Nebojsa Labus and Dr. Obrad Aleksic for useful discussions. This work was performed as part of projects III45007 and III45014 financed by the Ministry for Education, Science and Technological Development of the Republic of Serbia.

References

1. T. A. Blank, L. P. Eksperiandova, K. N. Belikov, Recent trends of ceramic humidity sensors development: A review, Sens. Actuators B 228 (2016) 416-442
2. H. Faharani, W. Wagiran, M. N. Hamida, Humidity sensors principle, mechanism and fabrication technologies: A comprehensive review, Sensors 14 (2014) 7881-7939
3. A. Mirzaei, B. Hashemi, K. Janghorban, "α-Fe_2O_3 based nanomaterials as gas sensors", J. Mater. Sci.: Mater. Electron., 27 (2016) 3109-3144
4. A. Sutka, K. A. Gross, Spinel ferrite oxide semiconductor gas sensors, Sens. Actuators B 222 (2016) 95-105
5. A. Tripathy, S. Pramqanik, A. Manna, S. Bhuyan, N. F. A. Shah, Z. Radzi, N. A. A. Osman, Design and development of capacitive humidity sensor applications of lead-free Ca,Mg,Fe,Ti-oxides-based electro-ceramics with improved sensing properties via physisorption, Sensors 16 (2016) 1135
6. G. Setz, N. Penin, L. Decoux, A. Wattiaux, M. Duttine, M. Gaudon, Near the ferric pseudobrookite composition, Inorg. Chem. 55 (2016) 2499-2507
7. W. Q. Guo, S. Malus, D. H. Ryan, Z. Altounian, Crystal structure and cation distributions in the $FeTi_2O_5$-Fe_2TiO_5 solid solution series, J. Phys. Condens. Matter 11 (1999) 6337-6346
8. Q. Liu, J. He, T. Yao, Z. Sun, W. Cheng, S. He, Y. Xie, Y. Peng, H. Cheng,Y. Sun, Yong Jiang, F. Hu, Z. Xie, W. Yan, Z. Pan, Z. Wu, S. Wei, Aligned Fe_2TiO_5-

containing nanotube arrays with low onset potential for visible-light water oxidation, Nat. Commun. 5 (2014) 5122
9. S. Petit, S. T. A. G. Melissen, L. Duclaux, M. T. Sougrati, T. Le Bahers, P. Sautet, D. Dambournet, O. Borkiewicz, C. Laberty-Robert, O. Durupthy, How should iron and titanium be combined in oxides to improve photoelectrochemical properties? J. Phys. Chem. C 120 (2016) 24521-24532
10. O. S. Aleksic, Z. Z. Vasiljevic, M. Vujkovic, M. Nikolic, N. Labus, M. Lukovic, M. V. Nikolic, Structural and electronic properties of screen printed Fe_2O_3/TiO_2 thick films and their photoelectrochemical behavior, J. Mater. Sci. 52 (2017) 5938-5953
11. M. V. Nikolic, M. D. Lukovic, Z. Z. Vasiljevic, N. J. Labus, O. S. Aleksic, Humidity sensing potential of Fe_2TiO_5-pseudobrookite, J. Mater. Sci.: Mater. Electron. 29 (2018) 9227-9238 DOI: 10.1007/s10854-018-8951-1
12. S. Ito, P. Chen, P. Comte, M. K. Nazeeruddin, P. Liska, P. Pechy, M. Graetzel, Fabrication of screen-printing pastes from TiO_2 powders for dye-sensitized solar cells, Prog. Photovolt. Res. Appl. 15 (2007) 603-612
13. B. H. Toby, R. B. Von Dreele, GSAS II the genesis of a modern open-source all purpose crystallography software package, J. Appl. Crystallogr. 46(2), 2013, 544-549
14. S. K Gautam, F. Singh, I. Sulania, R.G. Singh, P.K. Kulriya, E. Pippel, Micro-Raman study on the softening and stiffening of phonons in rutile titanium dioxide film: Competing effects of structural defects, crystallite size, and lattice strain, J. Appl. Phys. 115 (2014) 143504-1-5
15. Y. Hara, M. Nicol, Raman spectra and the structure of rutile at high pressures, Physica Status Solidi b 94 (1979) 317−322
16. B. Santara, P. K. Girl, K. Imakita, M. Fujii, Microscopic origin of lattice contraction and expansion in undoped rutile TiO2 nanostructures, J. Phys. D: Appl. Phys. 47 (2014) 215302
17. D. L. A. de Faria, S. V. Silva, M. T. de Oliveira, Raman microspectroscopy of some iron oxides and oxyhydroxydes, Journal of Raman Spectroscopy, 28 (1997), 873-878
18. Y.S. Li, J. S. Church, A. L.Woodhead, Infrared and Raman spectroscopic studies on iron oxide magnetic nano-particles and their surface modifications, J. Magn. Magn. Mater. 324 (2012) 1543–1550
19. D. Bersani, P. P. Lottici, A. Montenero, A micro-Raman study of iron-titanium oxides obtained by sol-gel synthesis, J. Mater. Sci. 35 (2000) 4301-4305
20. L. Wang, N. T. Nguyen, P. Schmuki, A facile surface passivation of hematite photoanodes with iron titanate cocatalyst for enhanced water splitting, ChemSusChem 9 (2016) 1-7
21. Y. Zhang, S. G. Ebbinghaus, A. Weidenkaff, T. Kurz, H.-A. Krug von Nidda, P. J. Klar, M. Guengerich, A. Reller, Controlled iron-doping of macrotextured nanocrystalline titania, Chem. Mater. 15 (2003) 4028-4033
22. S. Chen, Q. Zeng, J. Bai, J. Li, L. Li, L. Xia, B. Zhou, Preparation of hematite with an ultrathin iron titanate layer via an in situ reaction and its stable, long-lived, and excellent photoelectrochemical performance, Appl. Catalysis B: Environ. 218 (2017) 690-699
23. Y.-G. Lin, Y.-K. Hsu, Y.-C. Lin, Y.-C. Chen, Electrodeposited Fe_2TiO_5 nanostructures for photoelectrochemical oxidation of water, Electrochimica Acta 213 (2016) 898-903
24. Z. Lou, Y. Li, H. Song, Z. Ye, L. Zhu, Fabrication of Fe_2TiO_5/TiO_2 nanoheterostructures with enhanced visible-light photocatalytic activity, RSC Advances 6 (2016) 45343–45348

25. X. Zhu, J. Chen, X. Yu, X. Zhu, X. Gao, K. Cen, Controllable synthesis of novel hierarchical V_2O_5/TiO_2 nanofibers with improved acetone oxidation performance, RSC Advances 5 (2015) 30416–30424
26. Y. Luo, J Luo, J. Jiang, W. Zhou, H. Yang, X. Qi, H. Zhang, H. J. Fan, D. Y. W. Yu, C. M. Li, T. Yu, Seed assisted synthesis of highly ordered TiO_2@alpha-Fe_2O_3 core/shell arrays on carbon textiles for lithium-ion battery applications Energy Environ. Sci. 5 (2012) 6559-6566
27. G. Bhargava, I. Gouzman, C. M. Chun, T. A. Ramanarayanan, S. L. Bernasek, Characterization of the "native" surface thin film on a pure polycrystalline iron: A high resolution XPS and TEM study, Applied Surface Science 253 (2007) 4322-4329
28. J. Tauc, A. Menth, D. L. Wood, Optical and magnetic investigations of the localized states in semiconducting glasses, Phys. Rev. Lett. 25 (1970) 749-752
29. W. J. Lee, P. S. Shinde, G. H. Go, E. Ramasamy, Ag grid induced photocurrent enhancement in WO_3 photoanodes and their scale-up performance toward photoelectrochemical H_2 generation, Int. J. Hydrogen Energy 36 (2011) 5262-5270
30. P. S. Bassi, S. Y. Chiam, G. J. Barber, L. H. Wong, Hydrothermal grown nanoporous iron based titanate, Fe_2TiO_5 for efficient solar water oxidation, ACS Nano, 9 (2015) 5348-5356
31. S. Shinde, R. A. Bansade, C. H. Bhosale, K. Y. Kajpure, Physical properties of hematite α-Fe_2O_3 thin films: application to photoelectrochemical solar cells, J. Semiconductors 32(2011) 013001
32. B.-S. Jeong, D. P. Norton, J. D. Budai, Conductivity in transparent anatase TiO_2 films epitaxially grown by reactive sputtering deposition, J. Appl. Phys. 75 (1994) 2042
33. C.-L. Zhu, H.-L. Yu, Y. Zhang, T.-S. Wang, Q.-Y. Ouyang, L.-H. Qi, Y.-J. Chen, X.-Y. Xue, Fe_2O_3/TiO_2 tube-like nanostructures: synthesis, structural transformation and the enhanced sensing properties, ACS Appl. Mater. Interfaces, 4 (2012) 665-671
34. K. Momma, F. Izumi, VESTA 3 for three-dimensional visualization of crystal, volumetric and morphology data, J. Appl. Crystallogr. 44 (2011) 1271-1276
35. N. Agmon, The Grotthuss mechanism, Chem. Phys. Lett. 244 (1995) 456-462
36. J. Shah, R. K. Kotnala, B. Singh, H. Kishnan, Microstructure-dependent humidity sensitivity of porous $MgFe_2O_4$-CeO_2 ceramic, Sens. Actuators B 128 (2007) 306-311
37. P. Rao, R. C. Chikate, S. Bhagwat, Highly responsive and stable Y^{3+} doped NiMg-ferrite thick films as an efficient humidity sensor, New. J. Chem. 40 (2016) 1720-1728
38. P. M. Faia, C. S. Furtado, A. J. Ferreira, AC impedance spectroscopy: a new equivalent circuit for titania thick film humidity sensors, Sens. Actuators B 107 (2005) 353-359
39. A. S. Bondarenko, G. Ragoisha, EIS Spectrum Analyzer, http://www.abc.chemistry.bsu.by
40. M. V. Nikolic, D. L. Sekulic, Z. Z. Vasiljevic, M. D. Lukovic, V. B. Pavlovic, O. S. Aleksic, Dielectric properties, complex impedance and electrical conductivity of Fe_2TiO_5 nanopowder compacts and bulk samples at elevated temperatures, J. Mater. Sci.:Mater. Electron. 28 (2017) 4796-4806

Author biography

Maria V. Nikolic graduated at the Faculty of Electrical Engineering, University of Belgrade in 1990. She received a M.Sc. degree in electrical engineering in architecture and organization of computer networks in 1996 at the Faculty of Electronic Engineering, University of Belgrade. She obtained a Ph.D. degree in 2003 in materials science at the University of Belgrade. She is currently a research professor at the Institute for Multidisciplinary Research, University of Belgrade. Her current research interests include synthesis and characterization of oxide nanomaterials for humidity and gas sensors, thick film thermistors, sensors and devices based on them, photoelectrochemical cells, photocatalysts, ceramic and magnetic materials, sintering kinetics.

Zorka Z. Vasiljevic (formerly Djuric) obtained B. Sc. and masters' diploma in 2010 and 2011 at the Faculty of Technology and Metallurgy, University of Belgrade. She is currently working as research assistant at the Institute of Technical Sciences of SASA and is a Ph.D. student at the Faculty of Technology and Metallurgy, University of Belgrade. Her current interests include nanotechnology, synthesis and characterization of oxide materials for photoelectrochemical cells, photocatalysts and gas sensors, semiconductors and sintering.

Miloljub D. Luković was born on October 30, 1961. He received the B.S., M.S., and Ph.D. degrees in electrical engineering, all from University of Belgrade, Serbia, in 1988, 1993, and 2001 respectively. He is currently a research professor at the Institute for Multidisciplinary Research, University of Belgrade. His current research interests include experimental characterization of integrated thick-film LCV cells, thick film thermistors, sensors and devices based on them and EMI suppressors.

Vera P. Pavlovic is an Associate Professor at the Department of Physics and Electrical Engineering, Faculty of Mechanical Engineering, University of Belgrade. She is also one of the Regional Editors (for Europe) of the international journal "Science of Sintering". She graduated at the Faculty of Physics, University of Belgrade, received a M.Sc. degree in Materials Science at University of Belgrade and obtained a Ph.D. degree in Solid State Physics at the Faculty of Physics, University of Belgrade. Her current research interests refer to the field of polymer nanocomposites, nanotechnology and micro-ceramic materials, from the view point od synthesis-structure-properties relationship, primarily including the investigation of influence of mechanical activation, doping and other synthesis condition on: vibration (Raman, FTIR) and XPS spectra, sintering process, dielectric and ferroelectric properties, impedance spectra, opto-electronic and sensory effect, development of multiferroic nanomaterials, as well as development of hybrid films and nanostructures based on functionalized biopolymers, MWCNT and graphene.

Jelena Vujancevic graduated from the Faculty of Technology and Metallurgy, University of Belgrade, at the Department of Inorganic Chemical Technology. She enrolled in the doctoral studies in 2013 year at the Faculty of Technology and Metallurgy, the Department of Materials Engineering. She has been working at the Institute of Technical Sciences of SASA as a research assistant since April 2014. Her research interests include synthesis and characterization of nanomaterials, composite materials for photocatalysis, solar cells and photodetectros.

Milan Radovanovic is a Research Assistant Professor at the Faculty of Technical Sciences (FTS), University of Novi Sad (UNS), Novi Sad, Autonomous Province of Vojvodina,

Republic of Serbia. He received a MSc degree from the FTS-UNS in 2006, and a PhD degree from the FTS-UNS in 2016, all in electrical engineering. He is an author or co-author of 50 scientific papers including12 articles in leading international peer-reviewed journals. His research interest includes different type of sensors, characterization and testing of electronic materials, printed/organic/flexible electronics, etc. Milan Radovanovic has almost ten years of experience in working and implementation of different EU funded projects.

Jugoslav B. Krstic was born on October 28, 1968. He received the B.S., M.S., and Ph.D. degrees in Faculty of Physical Chemistry, all from University of Belgrade, Serbia, in 1999, 2007, and 2016 respectively. He is currently an associate research professor at the Institute of Chemistry, Technology and Metallurgy - Department of Catalysis and Chemical Engineering, University of Belgrade. His current research interests include synthesis and characterization of nanomaterials and catalysts and wide aspects of their application.

Branislav Vlahovic is professor of physics at NCCU and director of the Computational NSF Center of Research Excellence and NASA University Research Center for Aerospace Device. He obtained undergraduate and graduate degrees (nuclear physics and material science) in Zagreb University, Croatia. He was research scientist at Rudjer Boskovic Institute, Zagreb, from 1978 until 1990, when he moved to Duke University to work on low energy nuclear physics. Between 1996 and 2001 he had a shared appointment with Jefferson National Laboratory (medium energy nuclear physics) and NCCU. At NCCU he established material science, semiconductor physics, and nanotechnology laboratories and strong theoretical and experimental programs in material science and nuclear physics. For his research and work with students in 2004 he was awarded the Gardner award. He has published more than 200 peer reviewed articles in the fields of experimental and theoretical material science, nanotechnology, chemistry, cosmology, genomics, atomic, nuclear, and hypernuclear physics. His research interest are Nanotechnology, Chemistry, Cosmology, Genomics, Atomic,Nuclear, and Hypernuclear Physics.

Vladimir B. Pavlovic is professor of physics at the Department of Physics and mathematics, FoA, University of Belgrade and principal research fellow, Institute of Technical Sciences of the Serbian Academy of Sciences and Arts. He graduated at the Faculty of Physics, University of Belgrade, received a M.Sc. degree in Materials Science at University of Belgrade and obtained a Ph.D. degree in Solid State Physics at the Faculty of Physics, University of Belgrade. Vladimir B. Pavlovic established a laboratory for electron microscopy at FoA, University of Belgrade and strong theoretical and experimental research programs in the field of targeted synthesis of multifunctional materials at the Institute of Technical Sciences of the Serbian Academy of Sciences and Arts. His current research interests include research in the fields of prognosis of materials properties, development of smart eco and biomaterials, multiferroics, polymer nanocomposites, nanoceramics and sintering kinetics. He is the vice president of Serbian Ceramic Society and editor in chief of Science of Sintering.

Figure captions

Fig. 1 Pseudobrookite (Fe_2TiO_5) based thick film sample, alumina substrate with PdAg electrodes, SEM image of sample surface, FESEM image of cross-section of one printed thick film layer.

Fig. 2 Experimental setup.

Fig. 3 Rietveld analysis of the measured powder XRD pattern.

Fig. 4 Raman spectra of pseudobrookite based powder –blue, (P - pseudobrookite, A - anatase, R -rutile, H - hematite)Fe_2TiO_5 spectra from RRUFF database – grey, hematite spectra from RRUFF database – green, Raman spectra of starting anatase and hematite powder mixture –red and Raman spectra of anatase – black.

Fig.5 (a) Survey XPS spectra of pseudobrookite based powder; high resolution XPS spectra of: (b) Fe 2p, (c) Ti 2p, (d) O 1s; and (e) valence band spectra.

Fig. 6 Tauc plot for allowed indirect transition obtained from measured diffuse reflectance spectrum: inset First derivative analysis of diffuse reflectance spectrum and calculated values of transition energies.

Fig. 7 FESEM and TEM images of Fe_2TiO_5 based powder

Fig. 8 (a) SEM and (b) FESEM images of Fe_2TiO_5 based thick film sample surface.

Fig. 9 Change of impedance with frequency at (a) 25 and (b) 50^oC for different humidity values.

Fig. 10 Change of impedance at 25 and 50^oC with humidity at frequency of 42 and 101 Hz.

Fig. 11 Sensitivity of Fe_2TiO_5 based thick film samples calculated using eq. [1], insets show the sensor response calculated as $|Z|_a/|Z|_H$ at frequency of 42 Hz.

Fig. 12 Schematic illustration of the humidity sensing mechanism, FESEM image of microstructure, calculated band positions, pseudobrookite crystal structure drawn using VESTA [34].

Fig. 13 Response and recovery time of pseudobrookite based thick film sample at frequency of 100 Hz.

Fig. 14 Absorption and desorption curves obtained at 42 Hz for pseudobrookite based thick film samples at 25 and 50^oC.

Fig. 15 Complex impedance plots at (a) 25 (a) and (b) 50^oC.

Fig. 16 Change of (a) grain boundary resistance and (b) relaxation frequency with humidity.

Figure 1

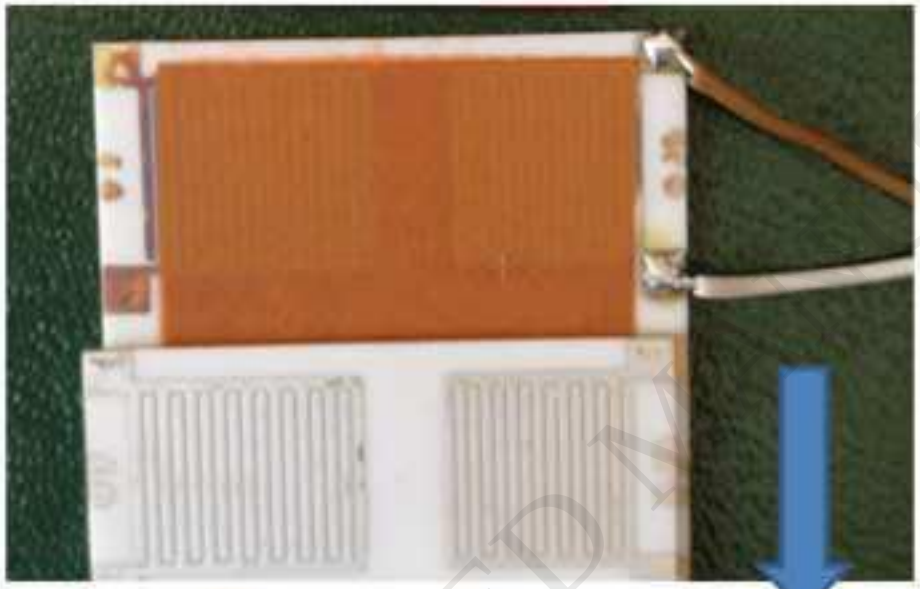

Fe_2TiO_5 thick film sample

Alumina substrate with PdAg electrodes

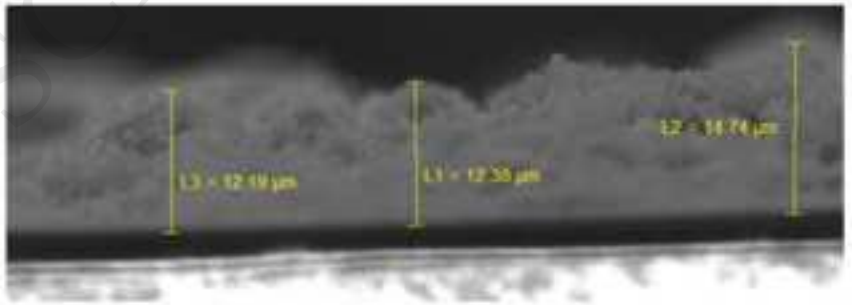

FESEM image of one screen printed thick film layer

Figure 2

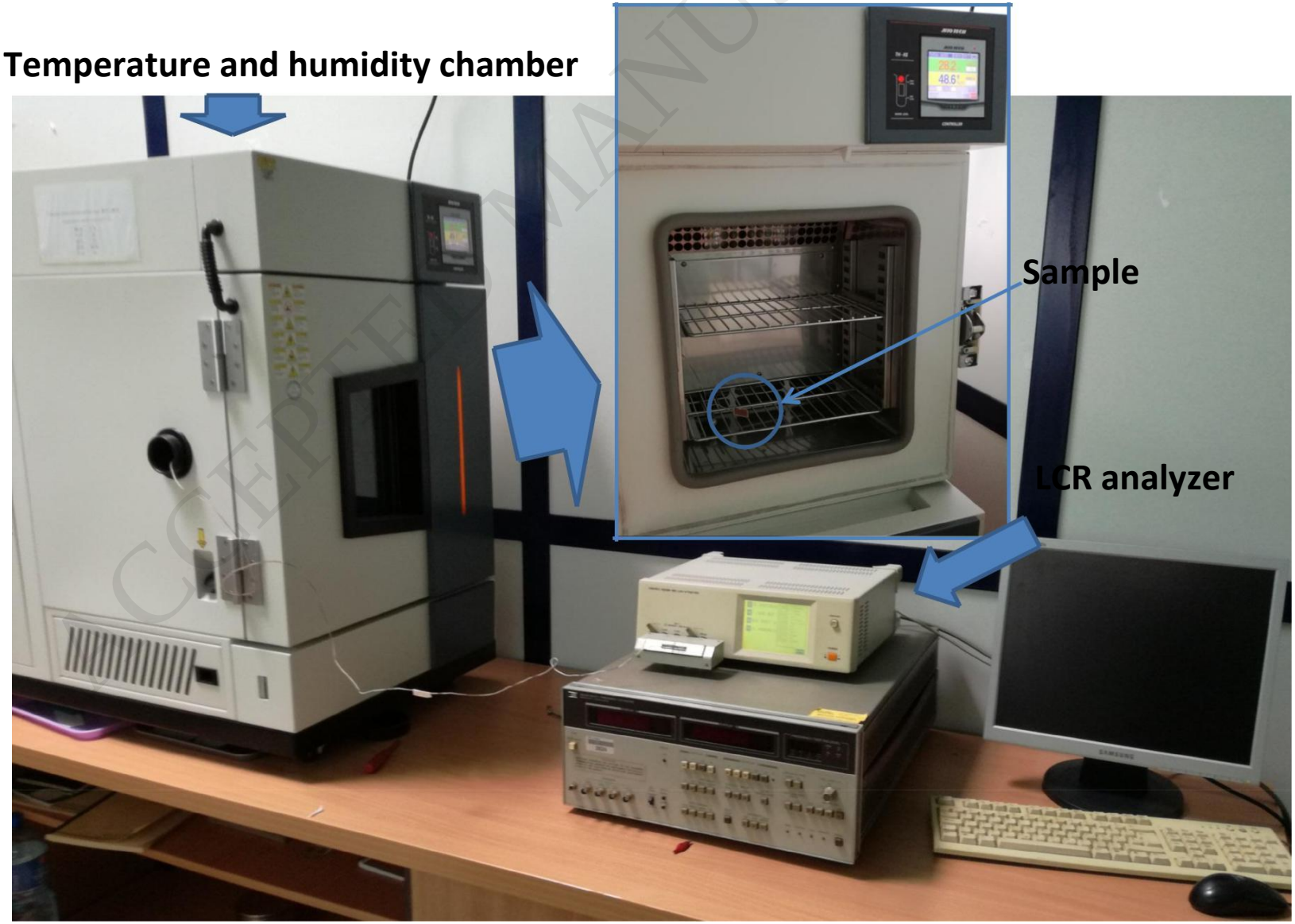

Figure 3

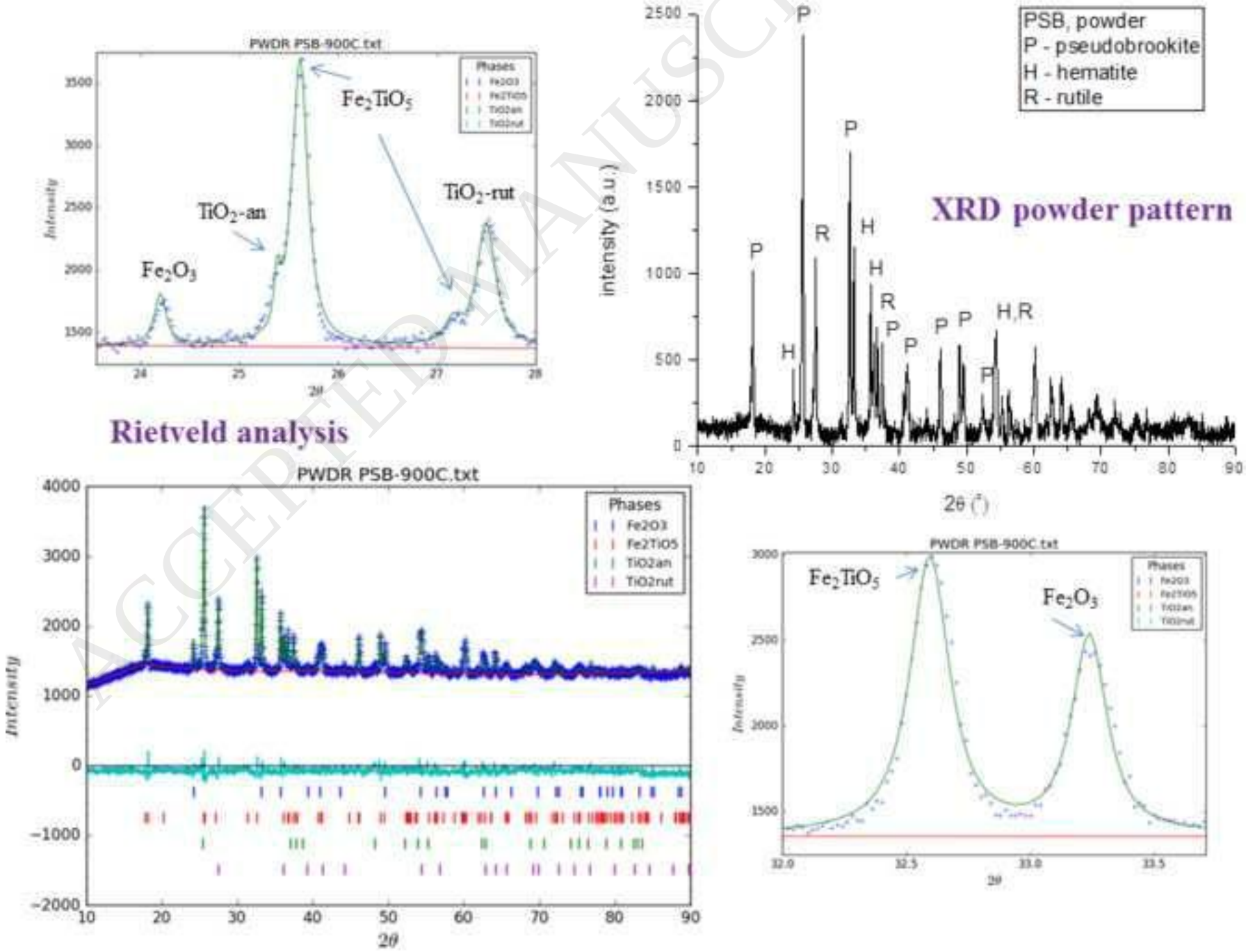

Figure 4

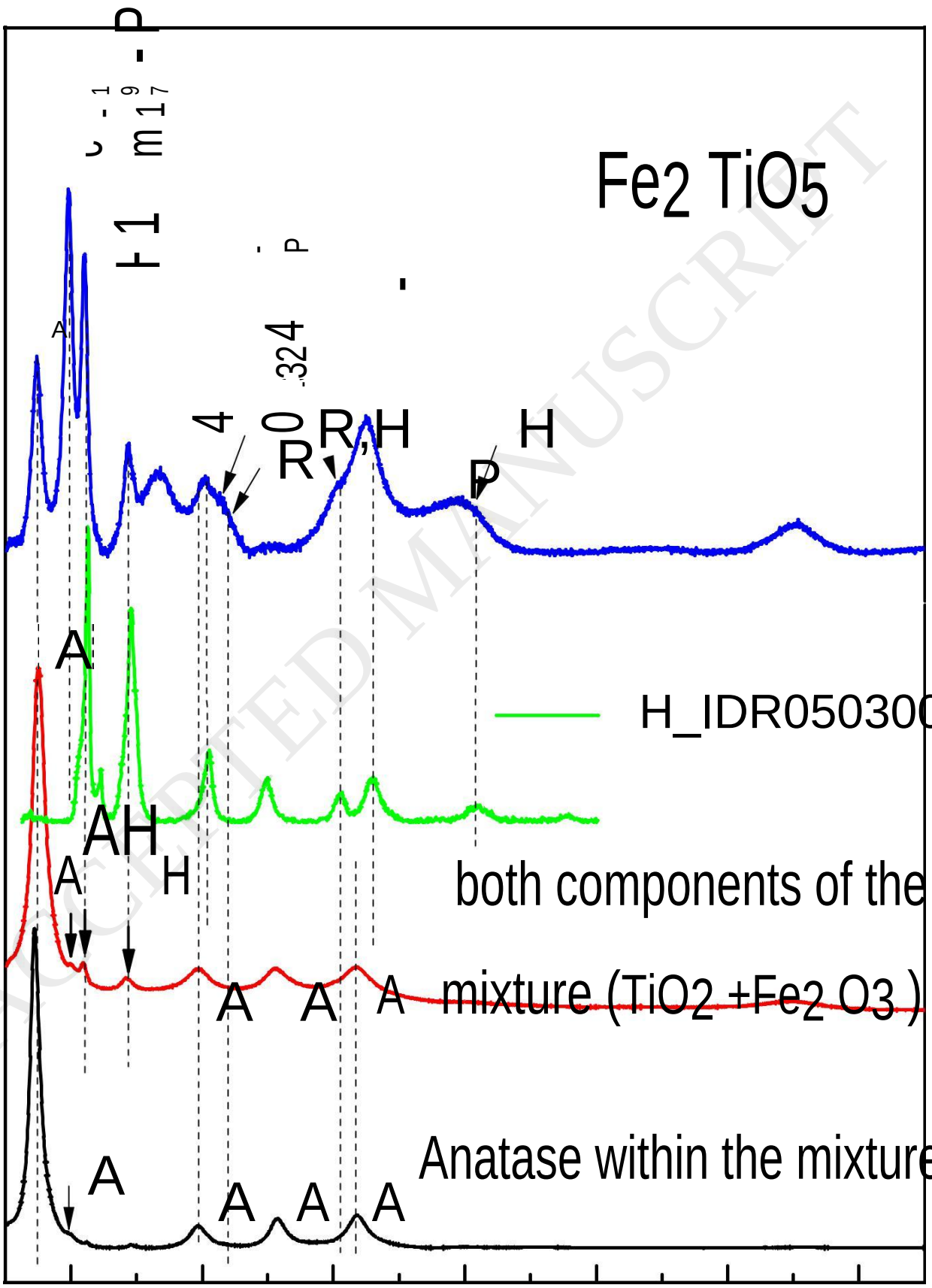

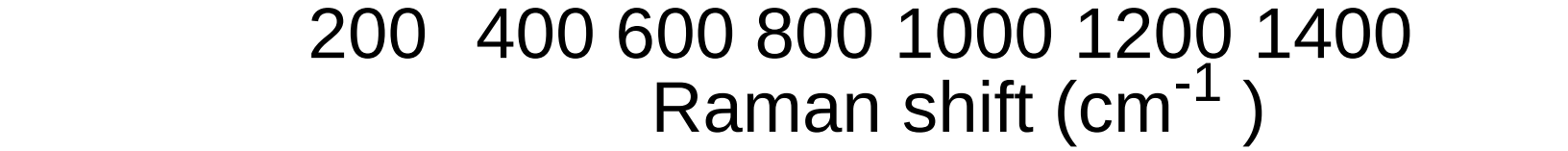

Figure 5

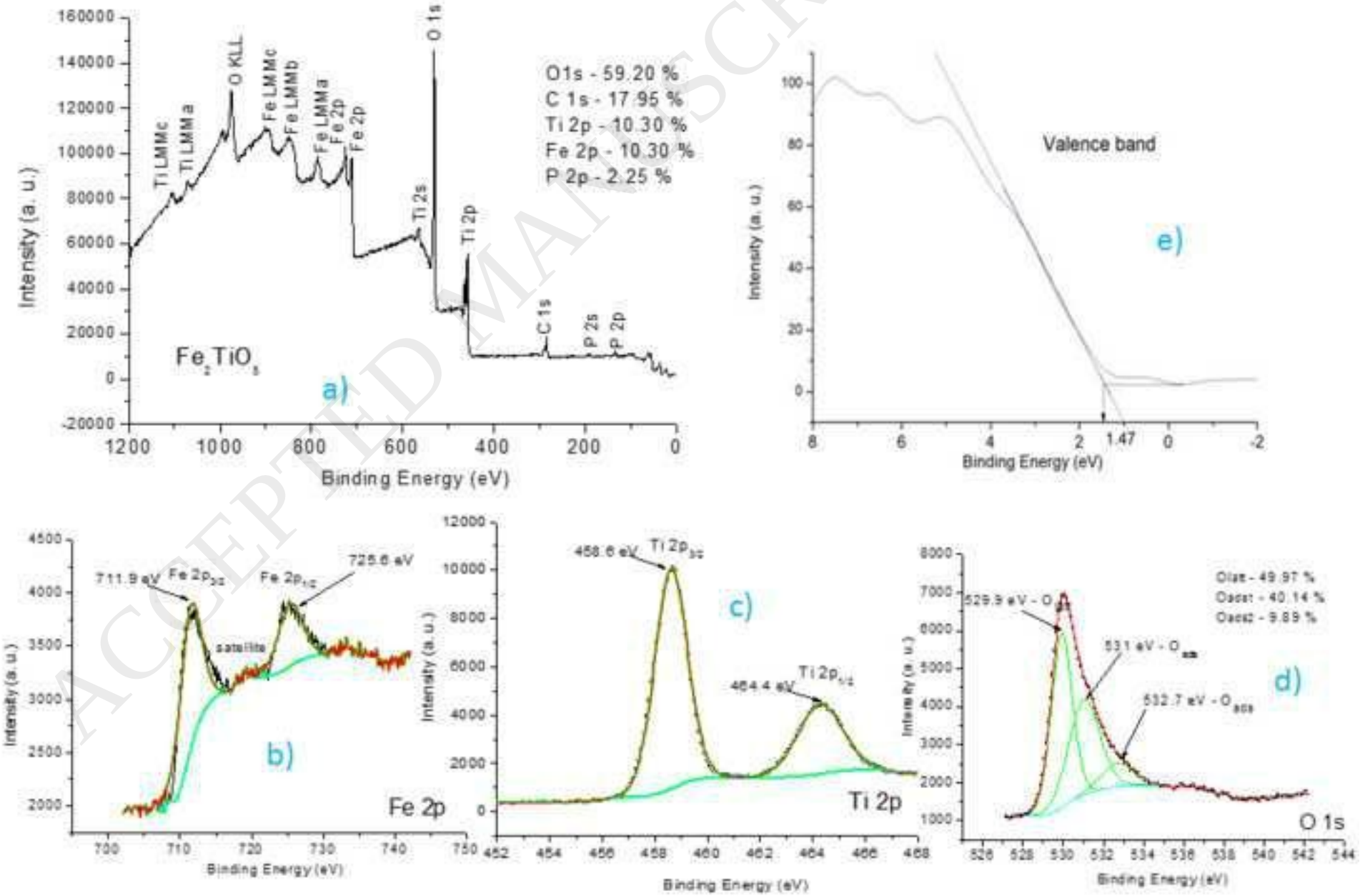

Figure 6

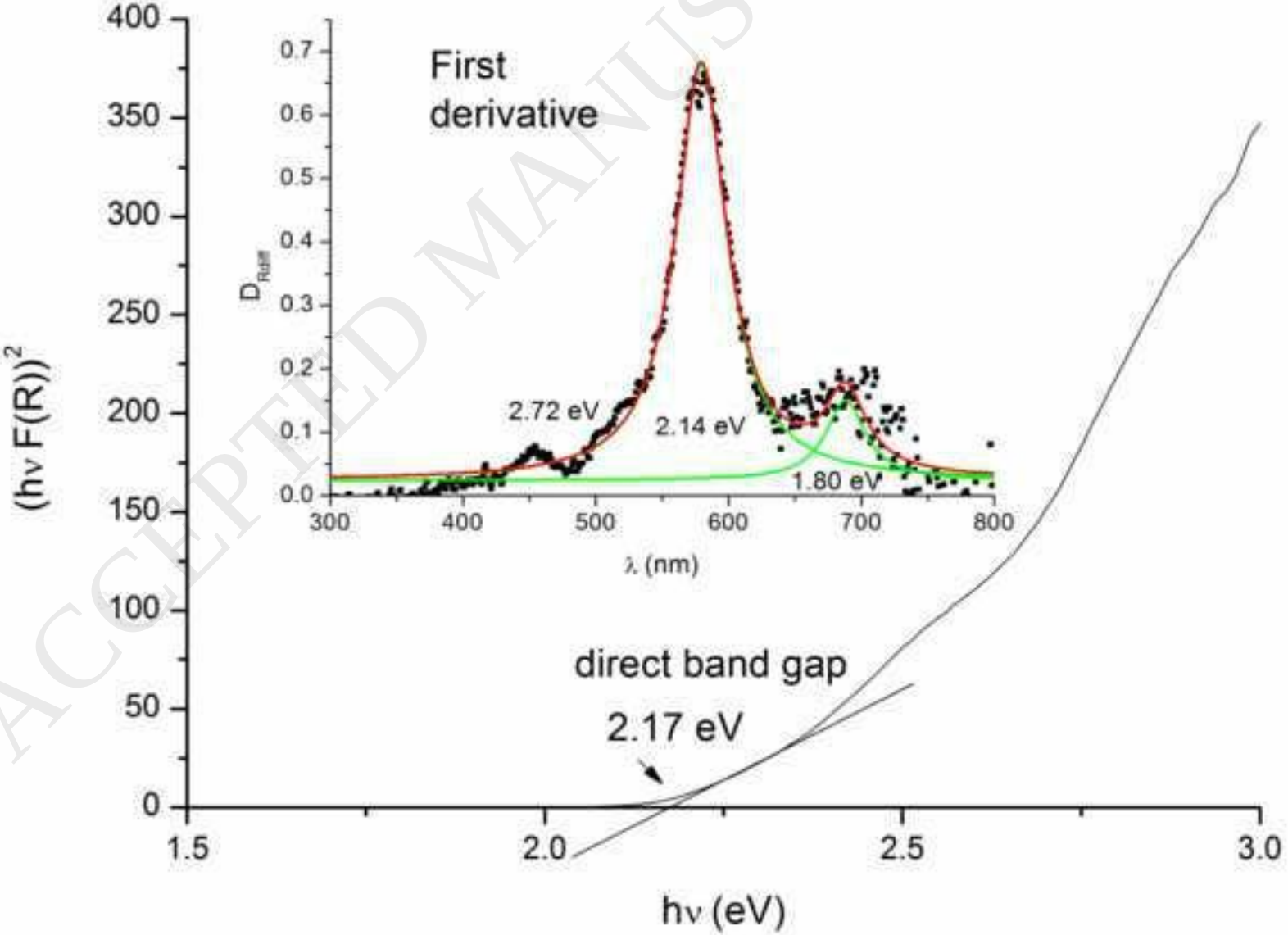

Figure 7

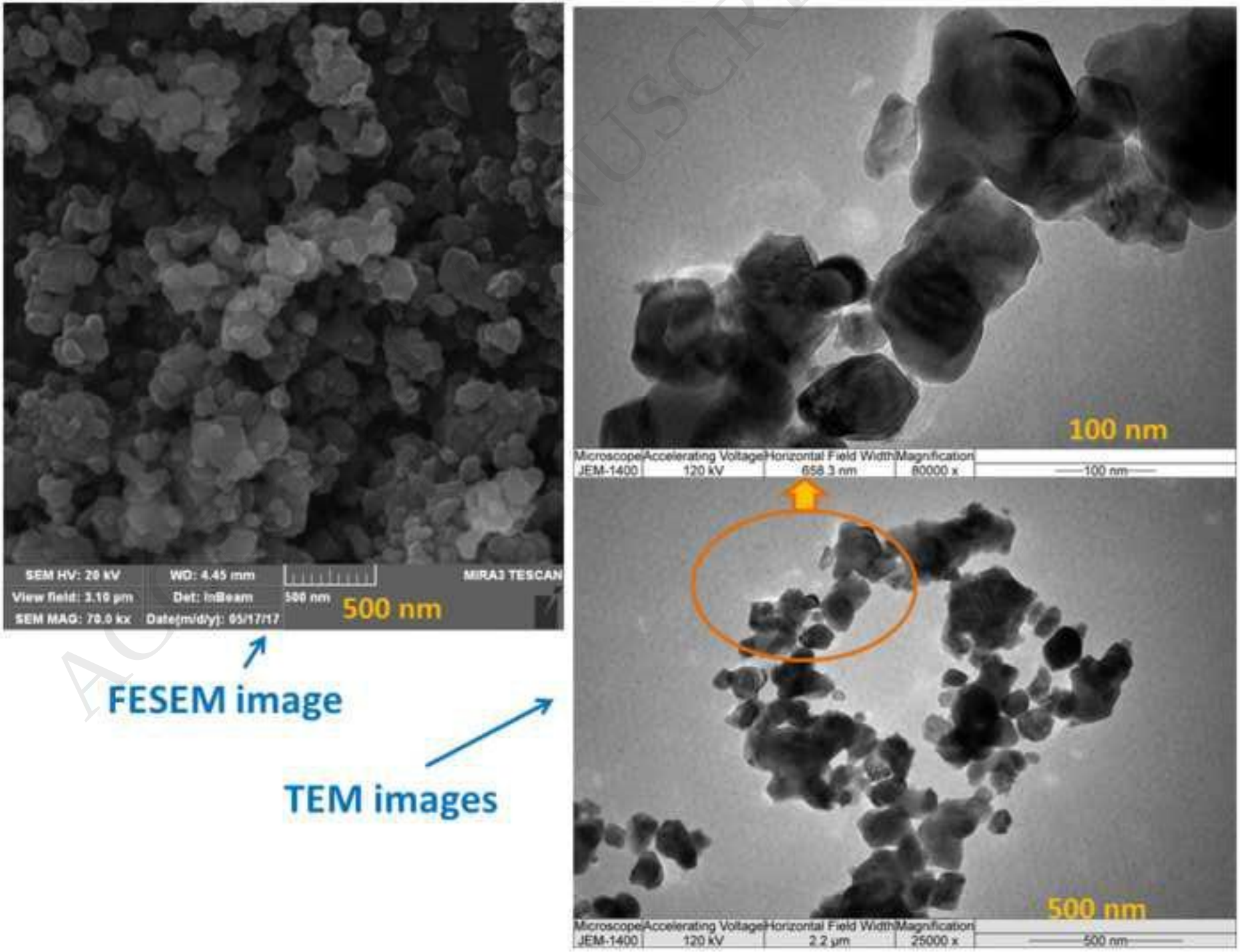
SEM HV: 20 kV
WD: 4.45 mm
MIRA3 TESCAN
View field: 3.10 µm
Det: InBeam
500 nm
SEM MAG: 70.0 kx
Date(m/d/y): 05/17/17
500 nm
FESEM image
TEM images
100 nm
Microscope Accelerating Voltage Horizontal Field Width Magnification
JEM-1400 120 kV 658.3 nm 80000 x 100 nm
500 nm
Microscope Accelerating Voltage Horizontal Field Width Magnification
JEM-1400 120 kV 2.2 µm 25000 x 500 nm

Figure 8

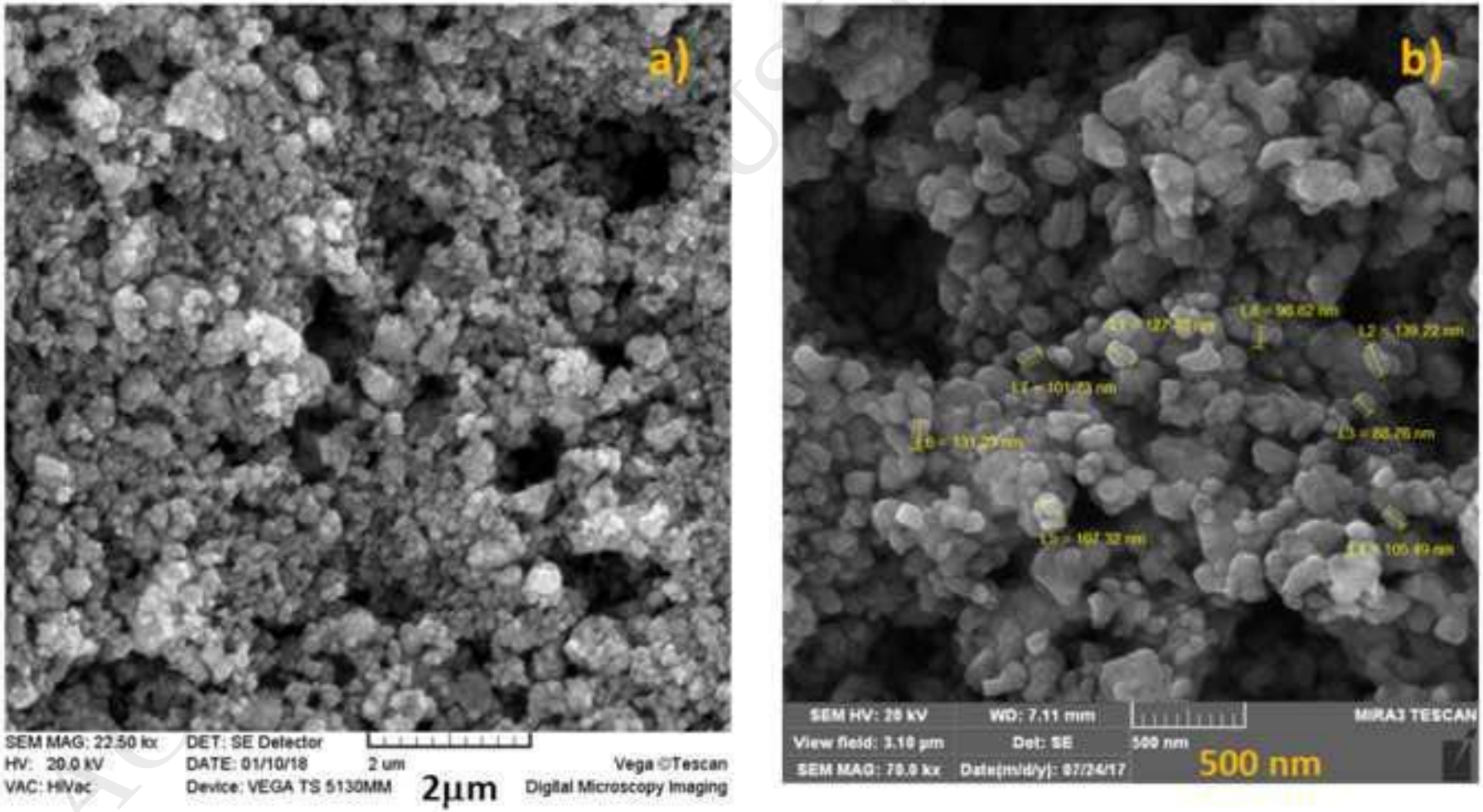
a)
SEM MAG: 22.50 kx
HV: 20.0 kV
VAC: HiVac
DET: SE Detector
DATE: 01/10/18
Device: VEGA TS 5130MM
2 um
2µm
Vega ©Tescan
Digital Microscopy Imaging
b)
SEM HV: 20 kV
WD: 7.11 mm
MIRA3 TESCAN
View field: 3.10 µm
Det: SE
500 nm
SEM MAG: 70.0 kx
Date(m/d/y): 07/24/17
500 nm

Figure 9a

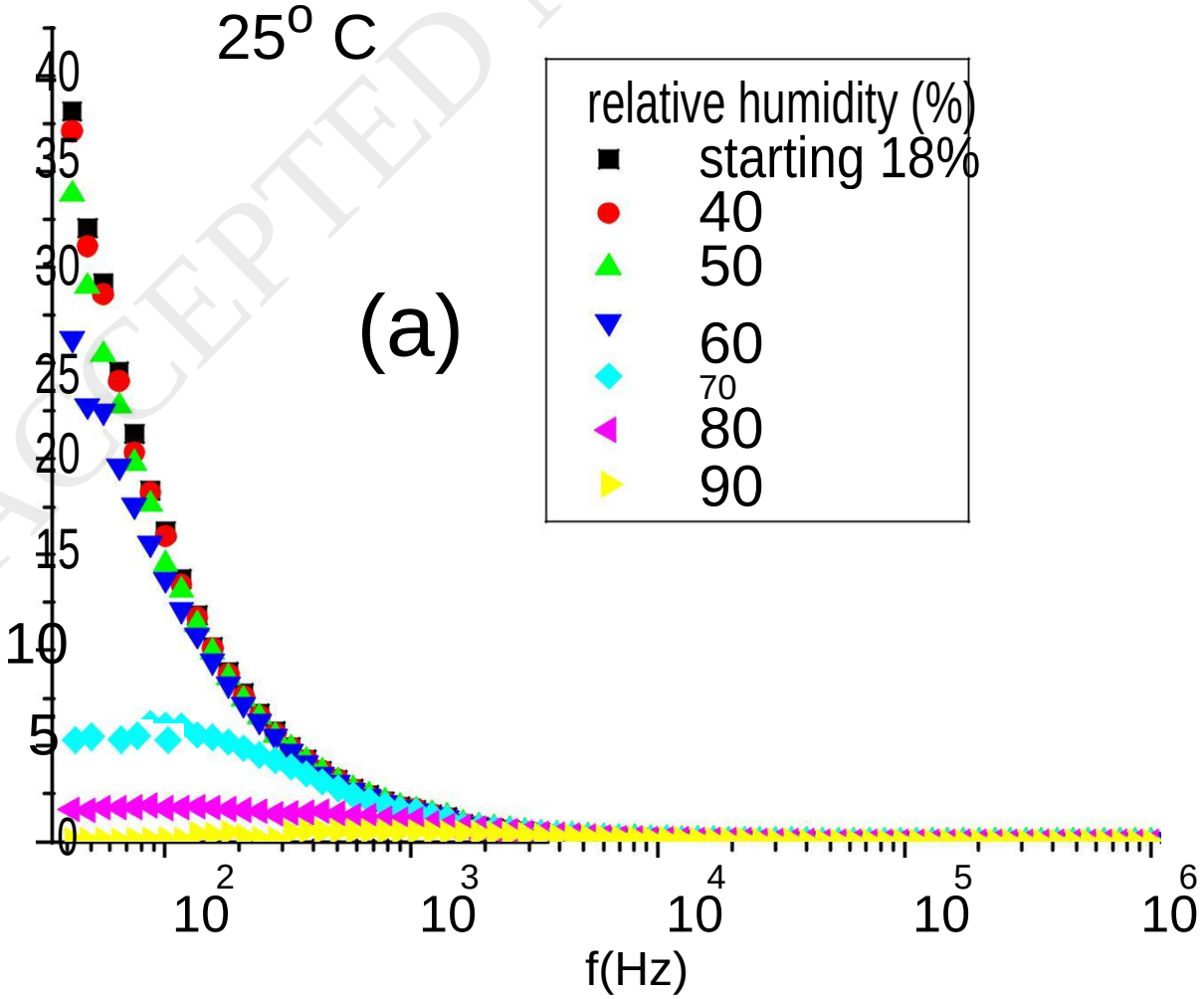

Figure 9b

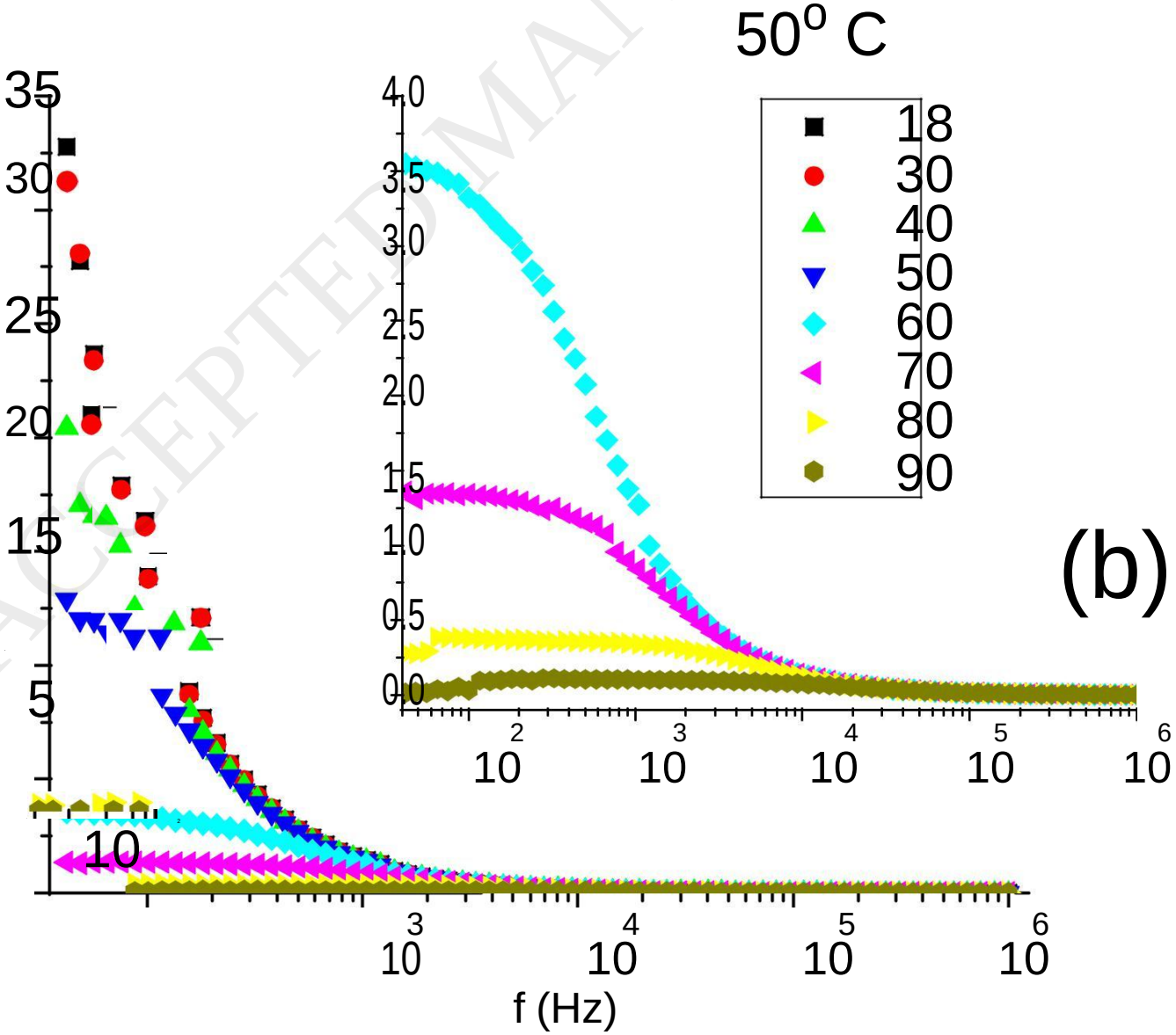

Figure 10

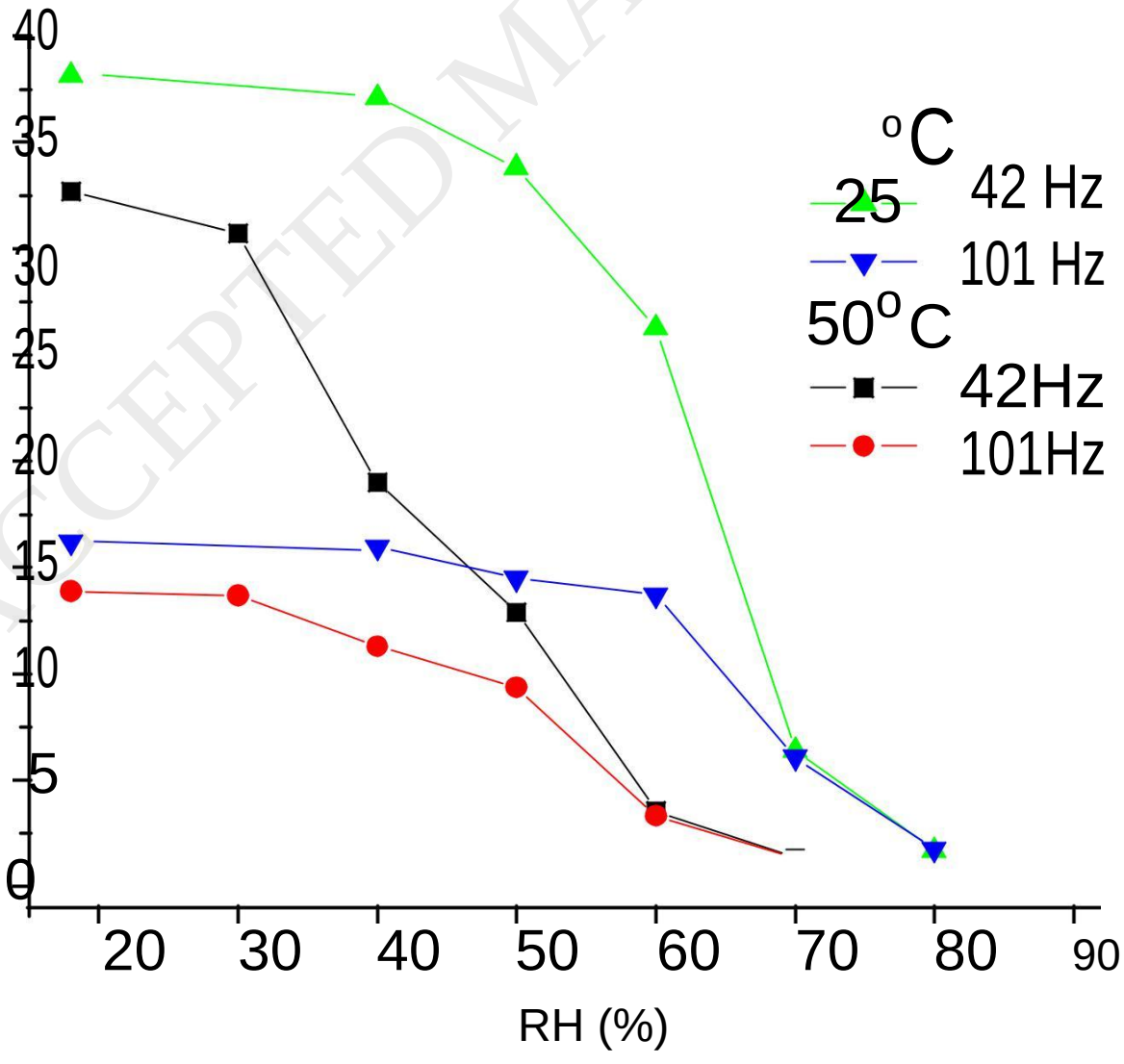

Figure 11

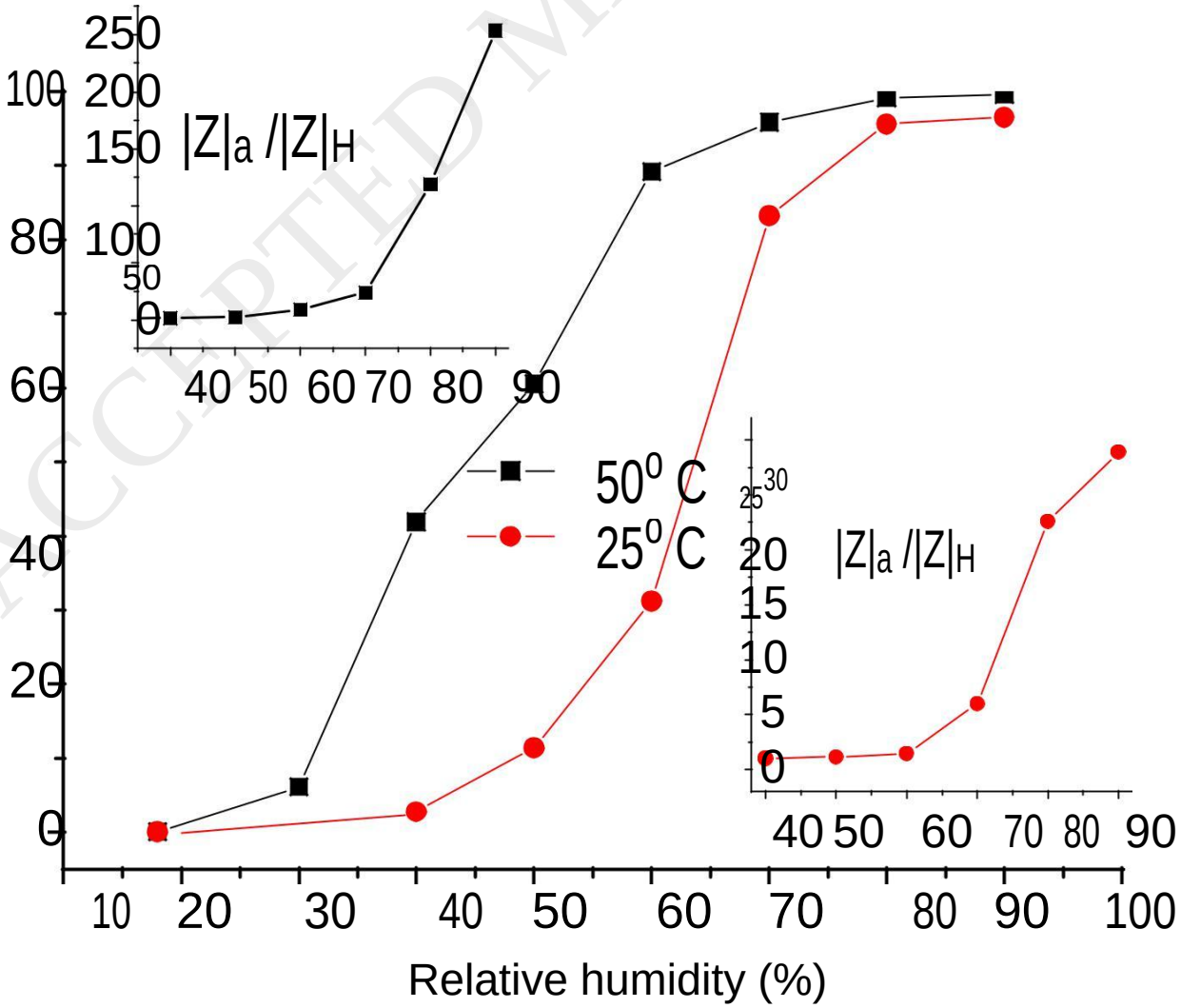

Figure 12

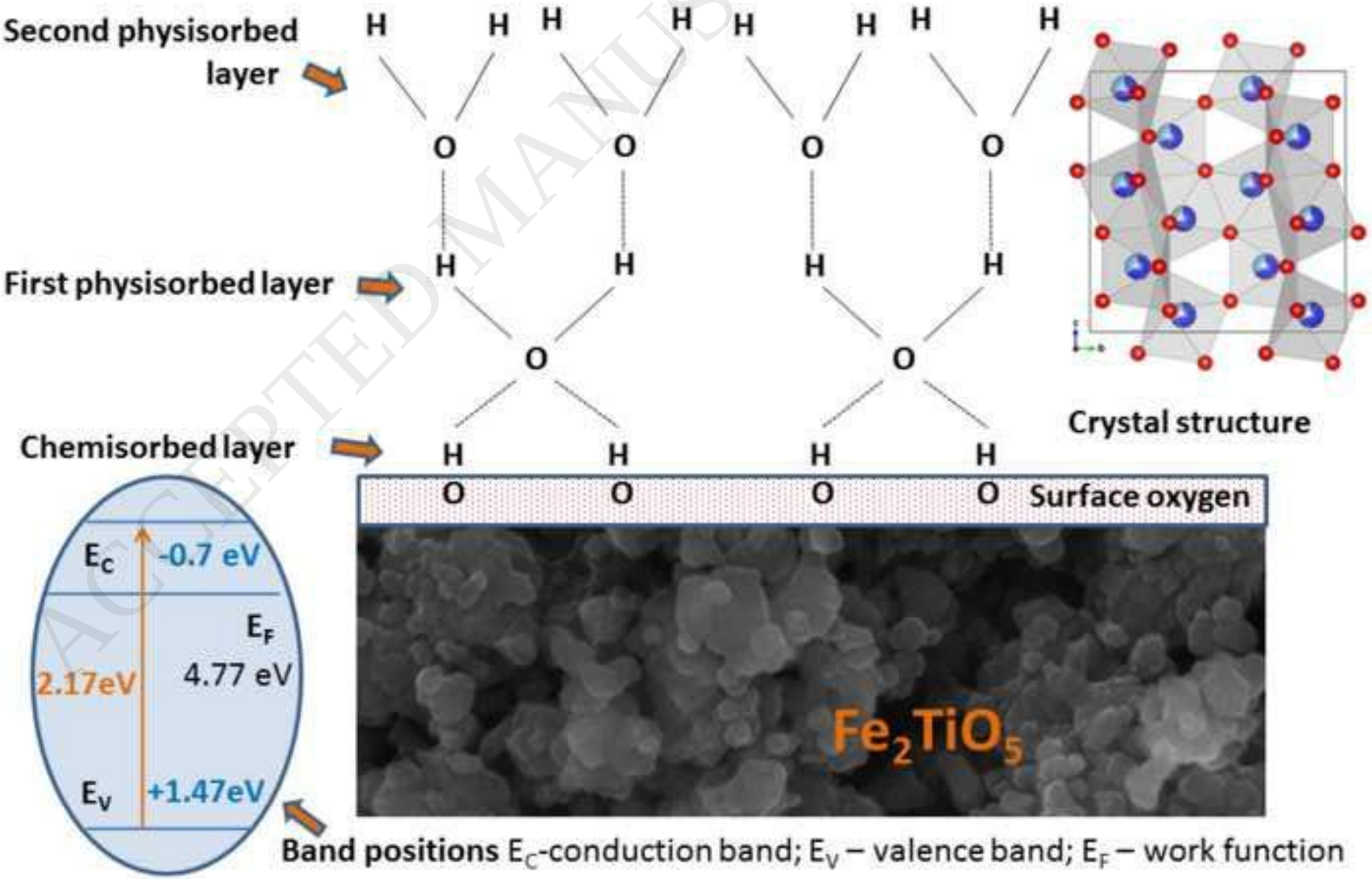

Figure 13

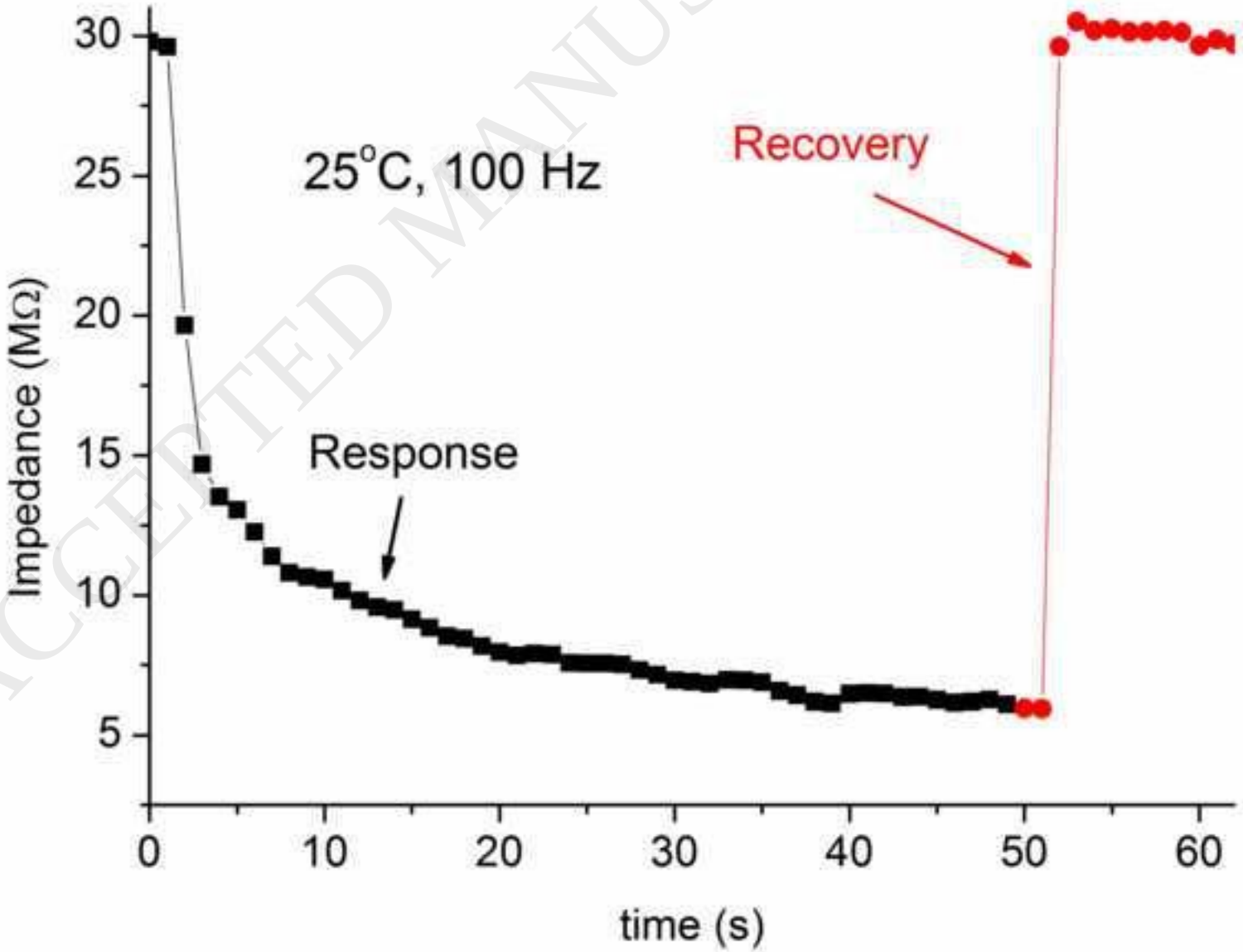

Figure 14

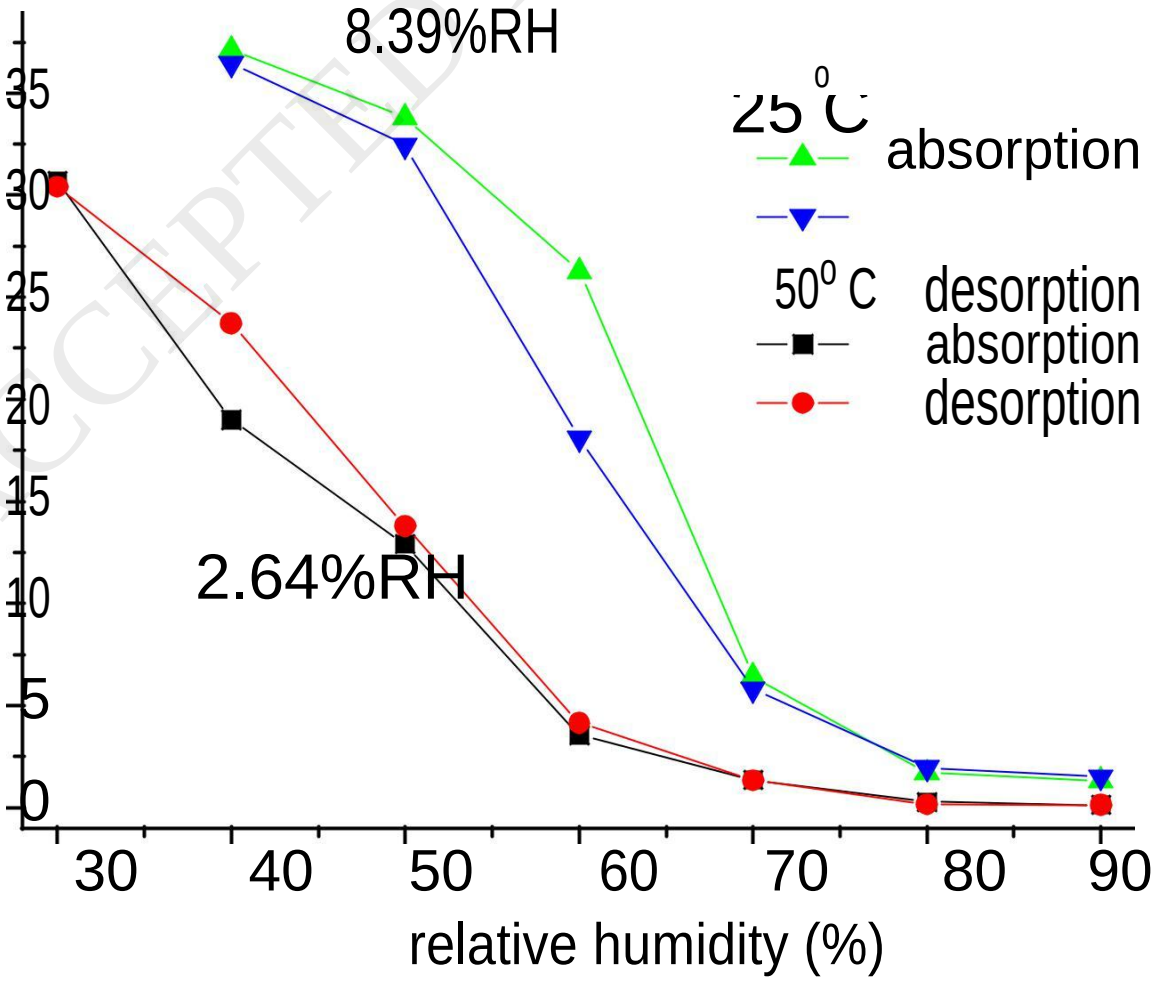

Figure 15a

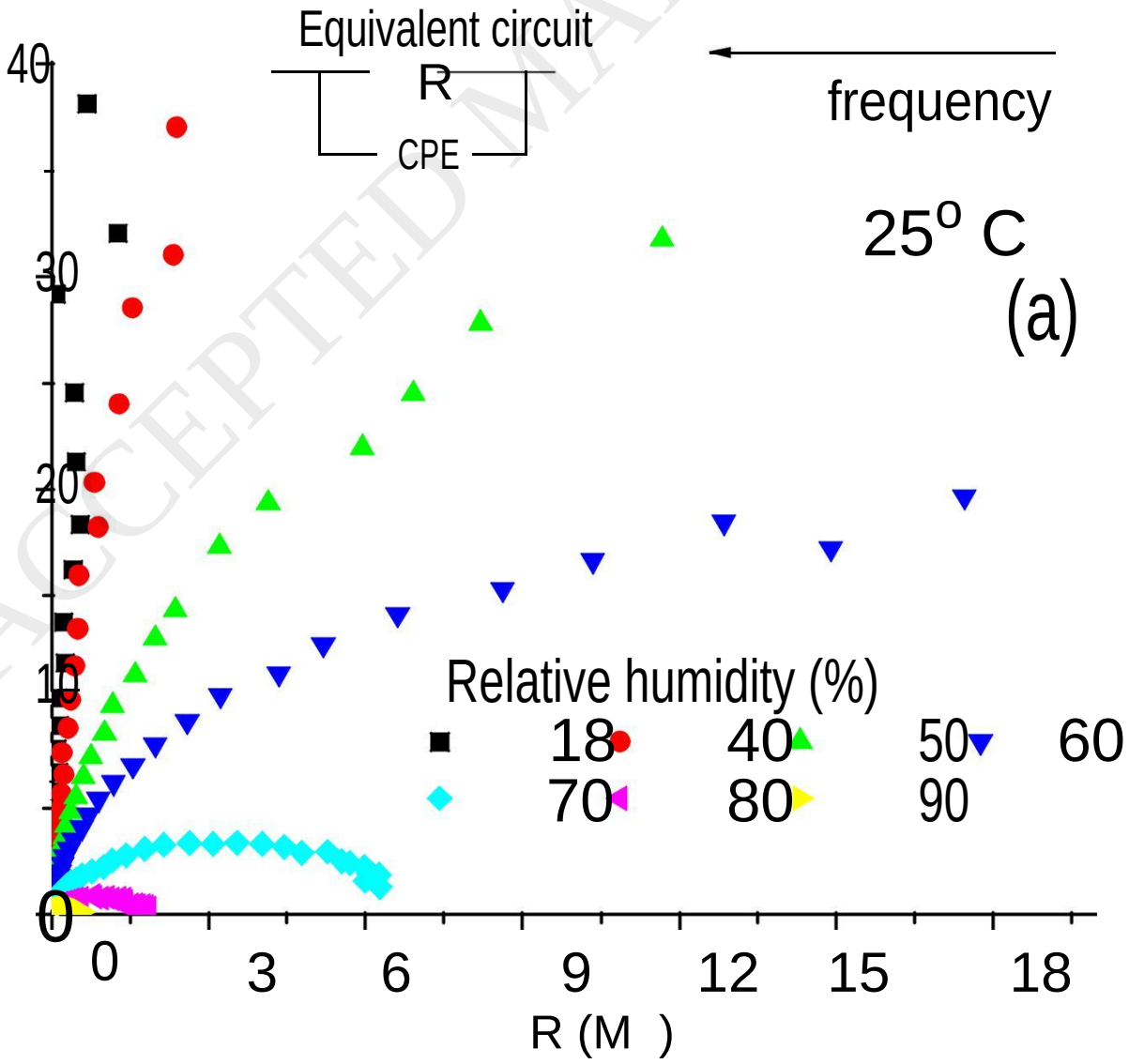

Figure 15b

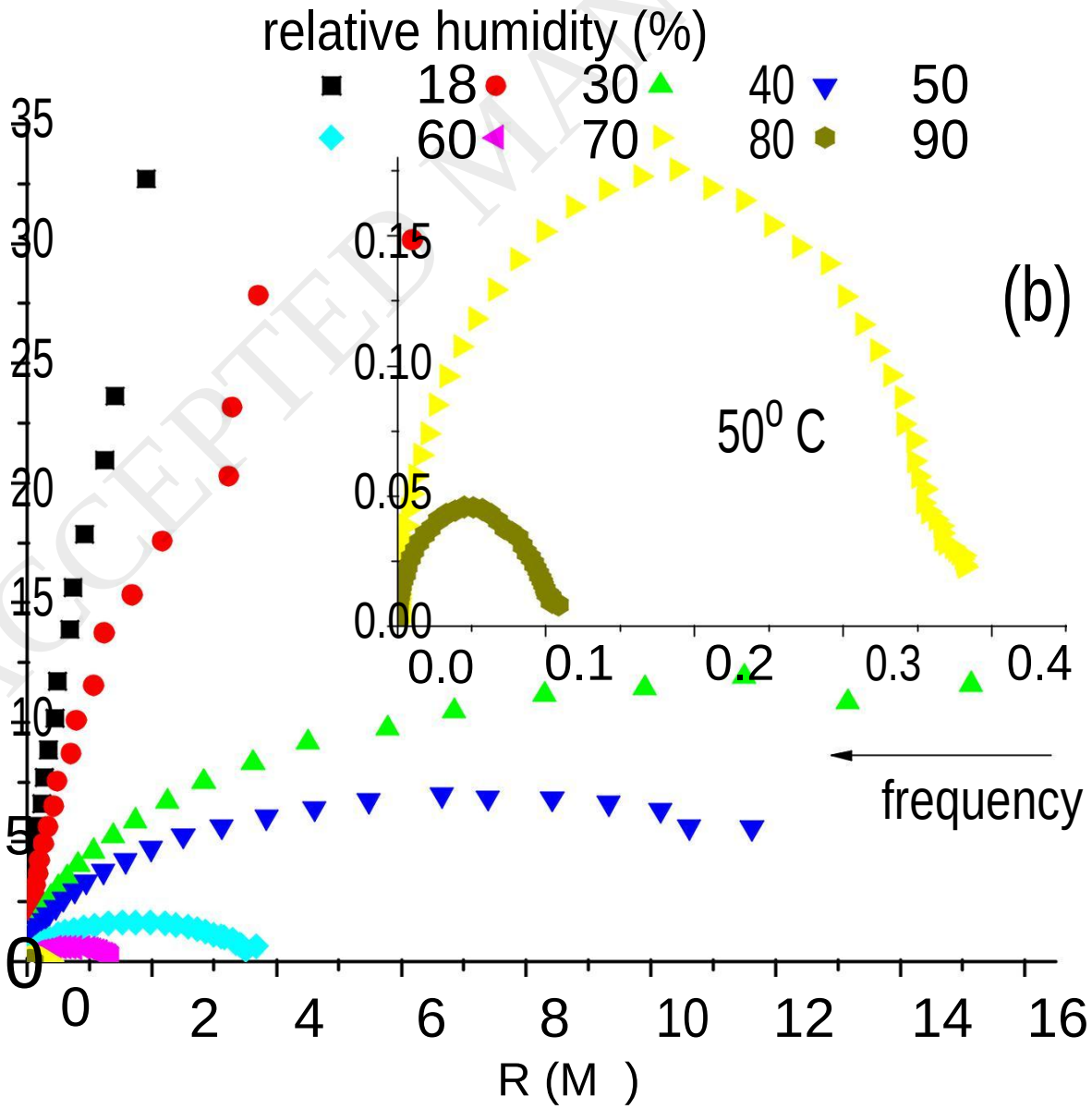

Figure 16a

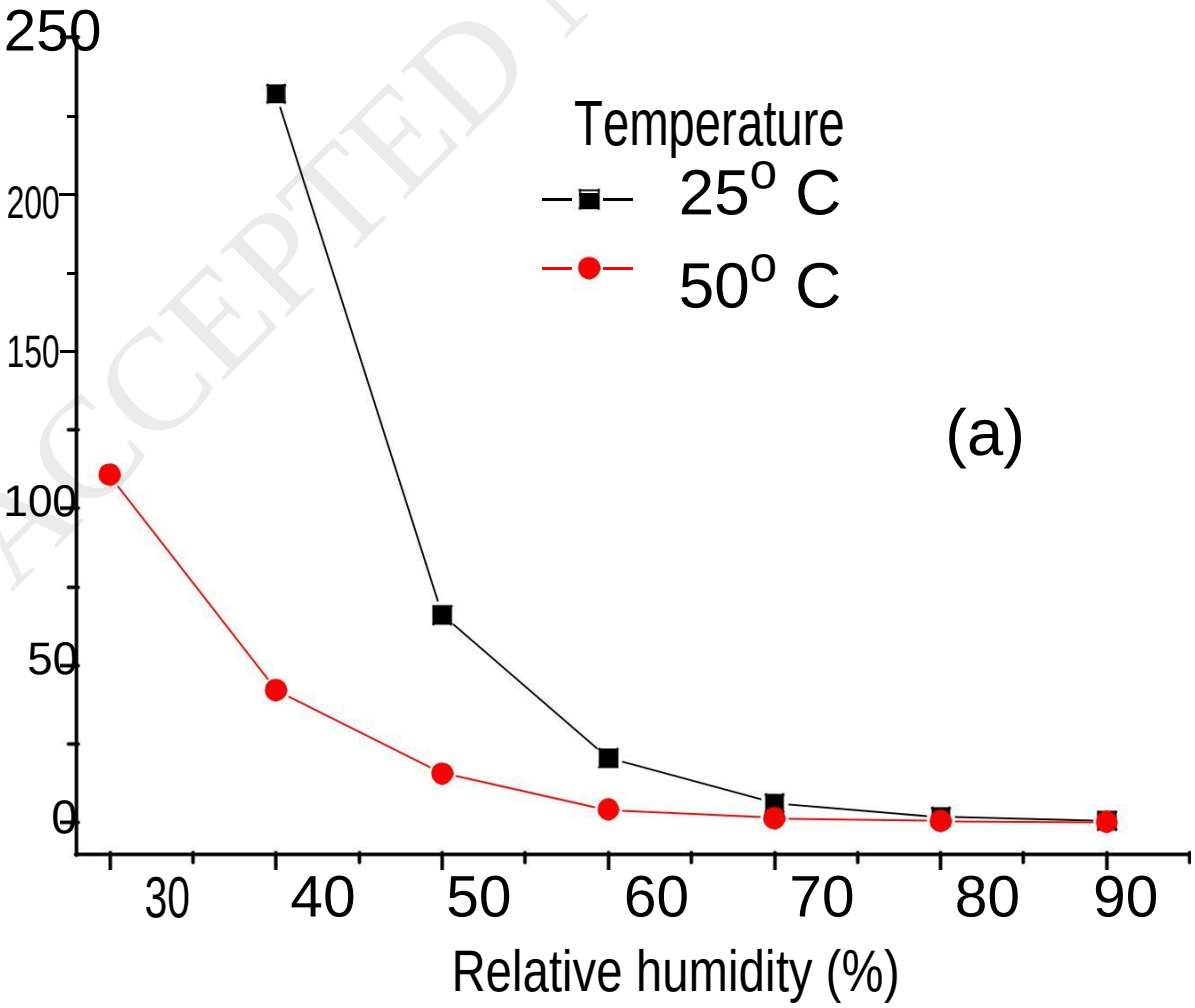

Figure 16b

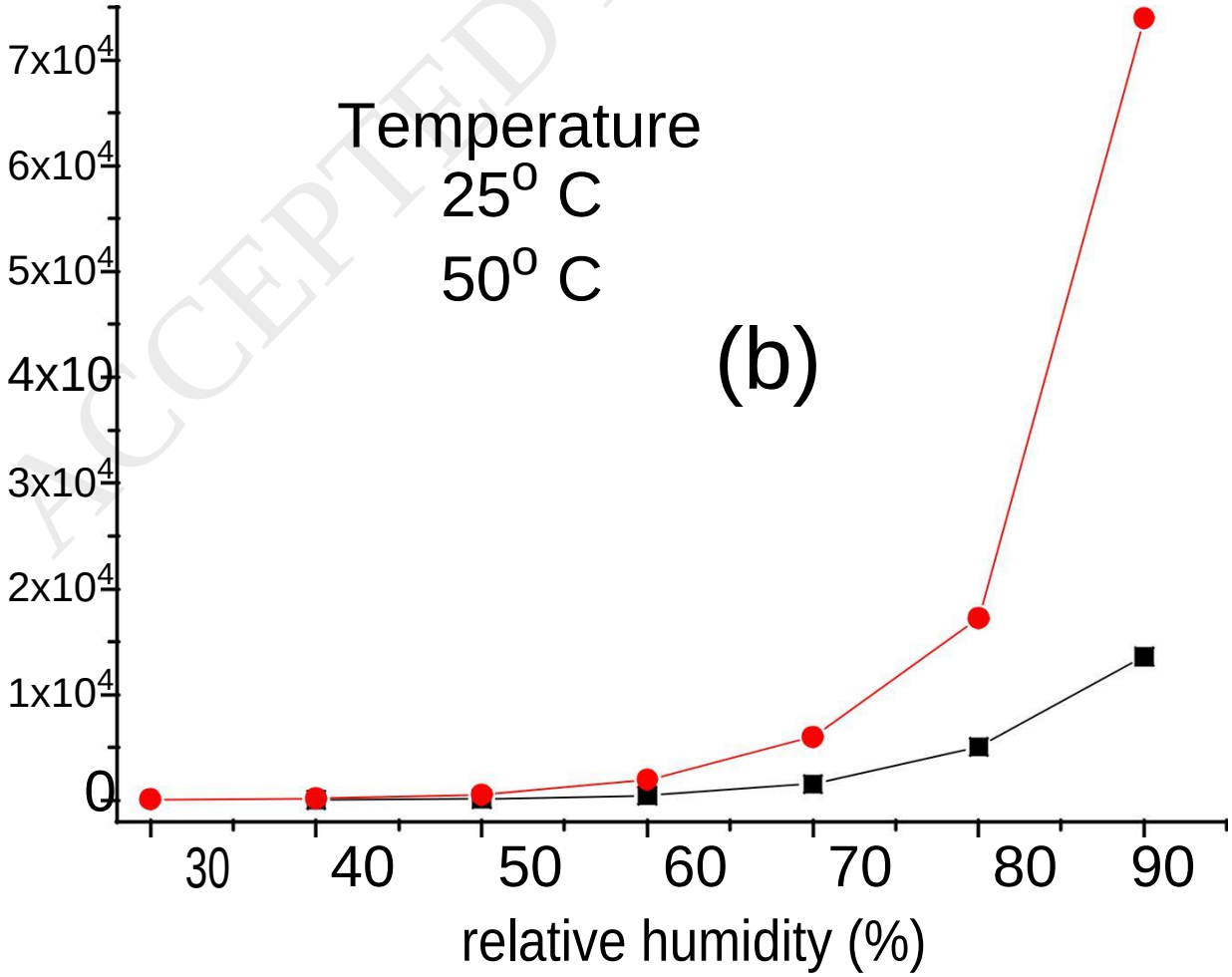

Table 1 Unit cell parameters for Fe_2TiO_5, TiO_2 (rutile and anatase) and Fe_2O_3 and atomic positions determined for Fe_2TiO_5

Table 1 Unit cell parameters for Fe_2TiO_5, TiO_2 (rutile and anatase) and Fe_2O_3 and atomic positions determined for Fe_2TiO_5

Pseudobrookite (Fe_2TiO_5), space group *Cmcm*, *a* = 3.7203(1), *b* = 9.7776(7), *c* = 9.9628(6) Å; crystallite size 42 nm, microstrain 1507.7						
atom	site	*x*	*y*	*z*	occupancy	U_{iso}
Fe1	8f	0.00000	0.1354(7)	0.5653(8)	0.6667	0.0160(25)
Ti1	8f	0.00000	0.1354(7)	0.5653(8)	0.3333	0.0160(25)
Fe2	4c	0.00000	0.1877(9)	0.25000	0.6667	0.016(4)
Ti2	4c	0.00000	0.1877(9)	0.25000	0.3333	0.016(4)
O1	4c	0.00000	0.770(3)	0.25000	1.000	0.039(12)
O2	8f	0.00000	0.0494(19)	0.1187(18)	1.000	0.012(8)
O3	8f	0.00000	0.3115(19)	0.0821(21)	1.000	0.016(7)
Hematite (Fe_2O_3) space group $R\bar{3}c$ *a* = *b* = 5.0295(8), *c* = 13.7244(14), crystallite size 245 nm, microstrain 6893.6						
Rutile (TiO_2) space group $P4_2/mnm$ with *a* = *b* = 4.5869(5), c = 2.9588(5) Å, crystallite size 46 nm, microstrain 1465.3						
Anatase (TiO_2), space group $I4_1/amd$ *a* = *b* = 3.7742(5), *c* = 9.519(3) Å						